# Water electrolysis

Shih, A.J.; Cecílio de Oliveira Monteiro, M.; Dattila, F.; Pavesi, D.; Philips, M.; Marques da Silva, A.H..; ... ; Koper, M.T.M.

# Water electrolysis

*Arthur J. Shih*[1,6,10]✉, *Mariana C. O. Monteiro*[1,7,10], *Federico Dattila*[2,8], *Davide Pavesi*[1], *Matthew Philips*[1], *Alisson H. M. da Silva*[1], *Rafaël E. Vos*[1], *Kasinath Ojha*[1,9], *Sunghak Park*[1], *Onno van der Heijden*[1], *Giulia Marcandalli*[1], *Akansha Goyal*[1], *Matias Villalba*[1], *Xiaoting Chen*[1], *G. T. Kasun Kalhara Gunasooriya*[3,4]✉, *Ian McCrum*[5]✉, *Rik Mom*[1]✉, *Núria López*[2]✉ *and Marc T. M. Koper*[1]✉

Abstract | Electrochemistry has the potential to sustainably transform molecules with electrons supplied by renewable electricity. It is one of many solutions towards a more circular, sustainable and equitable society. To achieve this, collaboration between industry and research laboratories is a must. Atomistic understanding from fundamental experiments and modelling can be used to engineer optimized systems whereas limitations set by the scaled-up technology can direct the systems studied in the research laboratory. In this Primer, best practices to run clean laboratory-scale electrochemical systems and tips for the analysis of electrochemical data to improve accuracy and reproducibility are introduced. How characterization and modelling are indispensable in providing routes to garner further insights into atomistic and mechanistic details is discussed. Finally, important considerations regarding material and cell design for scaling up water electrolysis are highlighted and the role of hydrogen in our society's energy transition is discussed. The future of electrochemistry is bright and major breakthroughs will come with rigour and improvements in the collection, analysis, benchmarking and reporting of electrochemical water splitting data.

Hydrogen evolution reaction (HER). The reaction at the cathode where hydrogen is produced.

Oxygen evolution reaction (OER). The reaction at the anode where oxygen is produced.

Alkaline electrolysis Water splitting under high-pH alkaline conditions. Although water splitting rates are lower under alkaline conditions, cell components exhibit higher resistance against corrosion and catalysts can be prepared from more earth-abundant materials.

✉*e-mail: arthur.shih@northwestern.edu; kasun.gunasooriya@ou.edu; imccrum@clarkson.edu; r.v.mom@lic.leidenuniv.nl; nlopez@iciq.es; m.koper@chem.leidenuniv.nl*

https://doi.org/10.1038/s43586-022-00164-0

With mounting concern over climate change[1,2] and a sharp decrease in the price of intermittent renewable electricity over the past few decades[3], electrochemistry is a promising solution in the challenging transition towards a renewable circular economy. This transition is poised to bring forth a more just and equitable society, albeit with important ethical, social and environmental complexities[4–7]. Hydrogen is ubiquitous in everyday life as it is used to refine petroleum, produce fertilizer, process foods and plastics and has a role in emerging markets in the transportation and utilities sectors. Administrations around the world have started pushing the research, development and commercialization of alternative hydrogen production pathways that emit little or no $CO_2$ (REFS.[8,9]) as more than 90% of hydrogen is currently produced from fossil fuels, contributing significantly to $CO_2$ emissions[10,11]. One promising pathway is electrochemical water splitting using renewable electricity (Eq. 1). In the absence of an electrochemical driving force, water exhibits an equilibrium between $H_2O$, hydrogen and oxygen, although this equilibrium highly favours water[12]. When an electrochemical driving force is applied, a thermodynamic minimum potential difference of 1.23 V at room temperature (298.15 K) is required to shift the equilibrium from $H_2O$ towards hydrogen and oxygen[13].

In electrochemical water splitting, hydrogen is formed at the cathode via a reaction called the hydrogen evolution reaction (HER) (Eqs. 2 and 4) and oxygen is formed at the anode via a reaction called the oxygen evolution reaction (OER) (Eqs. 3 and 5) (FIG. 1). Commercially, there are three low-temperature processes for the HER: alkaline electrolysis, proton exchange membrane (PEM) electrolysis and anion exchange membrane electrolysis. The best catalysts for the HER are noble metals, in particular platinum, whereas for the OER iridium and ruthenium oxides are the best candidate materials. There has been a large push towards developing catalysts using earth-abundant materials[14] because platinum, iridium and ruthenium are scarce, expensive and often mined via practices that exploit the environment and local populations[10,11,15]. Commercial alkaline water electrolysers employ nickel as a catalyst, at the expense of a lower efficiency compared with PEM devices for acidic water electrolysis.

$$\text{Water splitting}: H_2O \rightarrow H_2 + \frac{1}{2}O_2 \quad (1)$$

$$\text{HER in acid}: 2H^+ + 2e^- \rightarrow 2H_2 \quad (2)$$

$$\text{OER in acid}: 2H_2O \rightarrow O_2 + 4H^+ + 4e^- \quad (3)$$

$$\text{HER in base}: 2H_2O + 2e^- \rightarrow H_2 + 2OH^- \quad (4)$$

**Author addresses**

[1]Leiden Institute of Chemistry, Leiden University, Leiden, Netherlands.
[2]Institute of Chemical Research of Catalonia (ICIQ), The Barcelona Institute of Science and Technology (BIST), Tarragona, Spain.
[3]Department of Chemical, Biological and Materials Engineering, University of Oklahoma, Norman, OK, USA.
[4]Department of Physics, Technical University of Denmark, Kongens Lyngby, Denmark.
[5]Department of Chemical and Biomolecular Engineering, Clarkson University, Potsdam, NY, USA.
[6]Present address: Department of Materials Science and Engineering, Northwestern University, Evanston, IL, USA.
[7]Present address: Department of Interface Science, Fritz Haber Institute of the Max Planck Society, Berlin, Germany.
[8]Present address: Department of Applied Science and Technology (DISAT), Politecnico di Torino, Turin, Italy.
[9]Present address: Department of Chemistry and Biochemistry, University of Oregon, Eugene, OR, USA.
[10]These authors contributed equally: Arthur J. Shih, Mariana C. O. Monteiro.

$$\text{OER in base}: 4OH^- \rightarrow O_2 + 2H_2O + 4e^- \quad (5)$$

Low-temperature alkaline electrolysers have been on the market for more than 100 years, but are only responsible for around 4% of the total hydrogen production. PEM electrolysers have been commercialized for around 20 years, whereas anion exchange membrane electrolysers have only recently been deployed to industry. Still, the fundamental material and electrolyte properties that determine catalytic activity for the HER and OER are not yet well understood. In water electrolysis, the OER limits the overall water splitting rate[16]. Fundamental research in water electrolysis should focus on understanding stability, the fundamental mechanism and the impact of electrolyte species such as impurities. This focus would increase the efficiency of the electrolyser system as a whole, its operating life, power density and stack size, with the aim of reducing costs to make this technology more competitive.

This Primer overviews techniques and methods for water electrolysis and the intricacies of electrochemistry in aqueous media. It is assumed that the reader is adept in the fundamental concepts and theories of electrochemistry[17,18] and catalysis[19]. This Primer highlights best practices in five important areas of water electrolysis: catalyst preparation, characterization, kinetics, modelling and application. How these are key to disentangling problems in electrocatalysis research is emphasized, followed by the ever-growing importance of reproducibility and data deposition. Limitations and future opportunities of the field are also discussed.

## Experimentation

Important considerations when preparing electrochemical cells and electrodes for water electrolysis are discussed in this section. Additional challenges that arise when coupling electrochemical measurements with numerous characterization techniques are reviewed. To close off, advances that theory has provided to electrochemistry and catalysis are examined.

### *Electrochemical cell considerations*

***Cell design.*** Various electrochemical cells can be used to perform water electrolysis studies. The choice of cell should depend on factors including the type of electrode, product detection, electrolyte and whether it is coupled with a characterization technique. Batch cells (FIG. 2a) are mainly used in fundamental studies, where the focus lies in the voltammetric behaviour of electrode materials, as here the products of the working and counter electrodes are in the same compartment. It is easier to ensure cleanliness in these simple cells. H-cells (FIG. 2b) (H refers to the dual-chamber shape of the cell) have the counter and working electrode compartments separated by a membrane, which allows for product separation and more control over the catholyte/anolyte composition. The H-cell can be used with or without a pump to recirculate or refresh the electrolyte. Membrane electrode assembly cells (MEAs) (FIG. 2c) consist of a membrane, a catalyst and a flat plate electrode assembled together, and can be stacked to enable high productivity. MEAs can be found at different scales, from the laboratory bench (1 $cm^2$ electrodes) to industrial units (stacks of multiple 100 $cm^2$ electrodes), and are largely used in applied research. In the case of H-cells and MEAs, either PEMs or anion exchange membranes are used for acidic and alkaline electrolysers, respectively[20]. Both the cathode and the anode operate at the same pH, which may impose challenges in terms of electrode/catalyst stability. To operate using optimized pH conditions for the two different half-cell reactions (HER and OER), bipolar membranes (BPMs) can be used[21]. To date, commercial BPMs show considerable overpotentials for water dissociation within the BPM junction. Still, employing a catalyst in the BPM junction can significantly decrease overpotentials and enable the advance of BPM electrolysers[22].

When coupled with characterization or product detection techniques, electrochemical cells often need to be adapted. For example, special electrochemical cell configurations are used for in situ infrared spectroscopy (FIG. 2d), surface X-ray diffraction (FIG. 2e) and scanning tunnelling microscopy (STM) (FIG. 2f). Electrochemical cells are typically made of glass (batch, H-cell) or highly resistant polymers (MEAs). Considering that alkaline electrolytes can dissolve glass, polymer-based cells (typically polytetrafluoroethylene (Teflon), polyoxymethylene (Delrin), polypropylene or polyether ether ketone) should be employed when performing experiments in basic media[23–25]. Regardless of the type of cell employed, electrochemical cells and all parts that contact the electrolyte should be thoroughly cleaned prior to use, to remove contaminants that may affect the electrochemical signal[26–28] (BOX 1). Supplementary information Section 1.1 details a rigorous cleaning procedure that has provided reliable and reproducible results, with the impurities in chemicals used to clean cells summarized in Supplementary Table 1.

***Working electrode.*** Before contacting the electrolyte, electrodes must be systematically prepared to ensure cleanliness and reproducibility[29]. Most electrodes can be reused repeatedly, with their lifetime depending primarily on the reaction environment, the material and the geometry. Visual/microscopy inspection, reproducible cyclic voltammograms and reproducible catalytic currents are often used to ensure electrodes are cleaned and prepared sufficiently.

Proton exchange membrane
(PEM). A membrane selective towards protons ($H^+$), but not selective towards electrons (insulator) and gases (hydrogen, oxygen).

Anion exchange membrane
A membrane selective towards anions, but not selective towards electrons (insulator), gases (hydrogen, oxygen) and large cations.

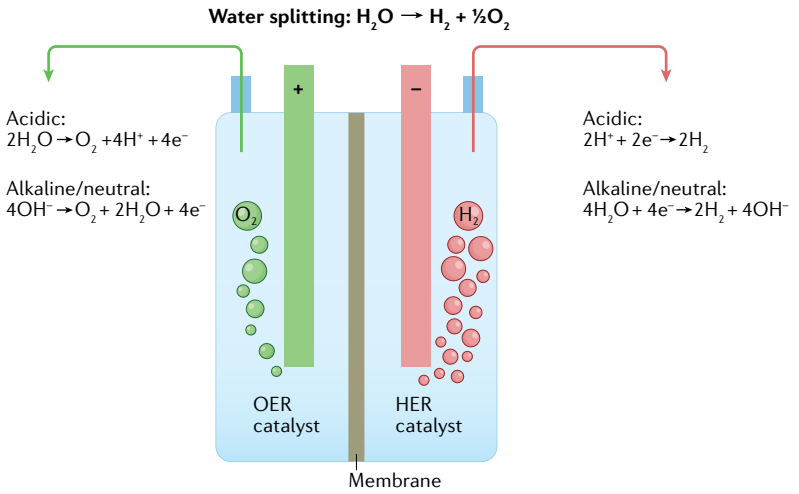


Fig. 1 |**Schematic of a typical water electrolyser.** Oxygen is produced at the anode (+) and hydrogen at the cathode (–). HER, hydrogen evolution reaction; OER, oxygen evolution reaction.

Electrodes are most commonly prepared by polishing to remove surface roughness, oxidized surfaces and inhomogeneities. The polishing media selected may strongly influence the outcome of measurements. The most common polishing paste and suspensions available are composed of alumina, diamond or silica. Alumina and diamond multifaceted particles remove material through a mechanical abrasive process. Silica, due to its spherical shape and high pH of the suspension, removes material through a chemo-mechanical process. The quality of polishing directly influences annealing effectiveness. Impurities may also be removed via electrochemical oxidation in concentrated acid at around 1–3 V, at the expense of introducing pits on the surface[30]. It has recently been shown that trace alumina left over from polishing can significantly impact the HER[31].

Polishing is not recommended for porous foam electrodes. Instead, sonication in organic solvents can remove organic contaminants, and sonication in acid and base can remove oxide and metallic impurities[29]. Care must be taken to ensure compatibility between the liquids and electrode as some materials can react or dissolve.

For metallic substrates, annealing is the most reliable way to obtain a clean and (re)ordered surface. Annealing can be performed using a butane torch open flame, or in a more controlled atmosphere using induction, especially for samples that are sensitive to air or require fine temperature control, such as copper and palladium, respectively[28,32]. In general, induction annealing leads to a more reproducible and cleaner surface. The annealing temperature will vary depending on the metal, and a comprehensive guide on the preparation and characterization of (single crystal surface) electrodes is available in the literature[33].

Once polished and cleaned, electrodes can be tested as is or active material can be deposited prior to further treatment and electrochemical testing. Drop casting and electrodeposition are two common methods to add active material such as porphyrins, nanoparticles or adatoms — sometimes in a layered structure to increase the active area[34,35]. The composition of the ink used for drop casting is important; Nafion is often used, but in some cases affects the performance[36–38]. Another critical factor in electrode preparation is control over the sample morphology. For example, even if the amount of material deposited on electrodes during drop casting is controlled, vastly different electrochemical results can be obtained depending on whether the material lumps together or is evenly spread out over the electrode[39].

***Counter electrode.*** Attention should be also given to the material and cleanliness of the counter electrode[40–43]. These can be homemade or commercial, and in the shape of coils, meshes or gauzes to ensure a large enough surface area (typically >10× the area of the working electrode). Counter electrodes can be cleaned in a similar way to the working electrode; for platinum, annealing in ambient air with a butane torch and etching in acid (such as nitric acid) is sufficient. In the case of experiments drawing high current densities, or using transition metals, alloys and other catalysts, either an inert counter electrode such as graphite should be used or the counter electrode compartment must be separated using a membrane to minimize cross-contamination that can come from its dissolution[41,43]. It was recently demonstrated that Nafion membranes are unable to completely prevent the transport of metal ions to a carbon working electrode[43]. Thus, convincing evidence that non-precious HER catalysts do not contain contamination from leached precious metals from the counter electrode must be shown. Care must also be taken as carbon counter electrodes can potentially oxidize to CO and $CO_2$ at high enough potentials; CO can poison both the counter and working electrodes[44]. Dimensionally stable anodes are considered the best counter electrode candidates for the OER, especially to ensure stability in acidic media[42]. In the case of the HER, high surface area platinum is still considered the best candidate.

***Reference electrode.*** The choice of a reference electrode should depend on the electrolyte composition and pH[45]. Reference electrodes sheathed in glass, for instance, should not be employed for experiments in alkaline media, as dissolution may introduce undesired cationic species into the electrolyte[23–25]. Reference electrodes should be validated and refilled often, as shifts in the standard equilibrium potential can happen after storage[46]. Malfunction of an Ag/AgCl electrode can lead to $Ag^+$ and $Cl^-$ leakage into the electrolyte[47,48]. During water electrolysis, $Ag^+$ ions can electrodeposit onto the cathode, and $Cl^-$ ions can strongly bind to the anode and compete with water oxidation forming $Cl_2$. The most reliable reference electrode is hydrogen bubbled through a platinum wire or mesh in a hydrogen-saturated electrolyte separated from the main electrolyte via a Luggin capillary[49,50], also known as the reversible hydrogen electrode (RHE). It is highly recommend either to use the pH-dependent RHE directly as a reference electrode or to calibrate other pH-independent electrodes[46,50]. A comprehensive technical note is available from ASL Co. and can be used not only for choosing an appropriate reference electrode but also for learning its limitations (reference electrode technical note).

Dimensionally stable anodes
Conductive and stable electrodes made of mixed metal oxides (typically of titanium, ruthenium and iridium).

Reversible hydrogen electrode
(RHE). A reference electrode defined as the equilibrium potential of platinum when exposed to 1 atm hydrogen and the pH of the working electrolyte.

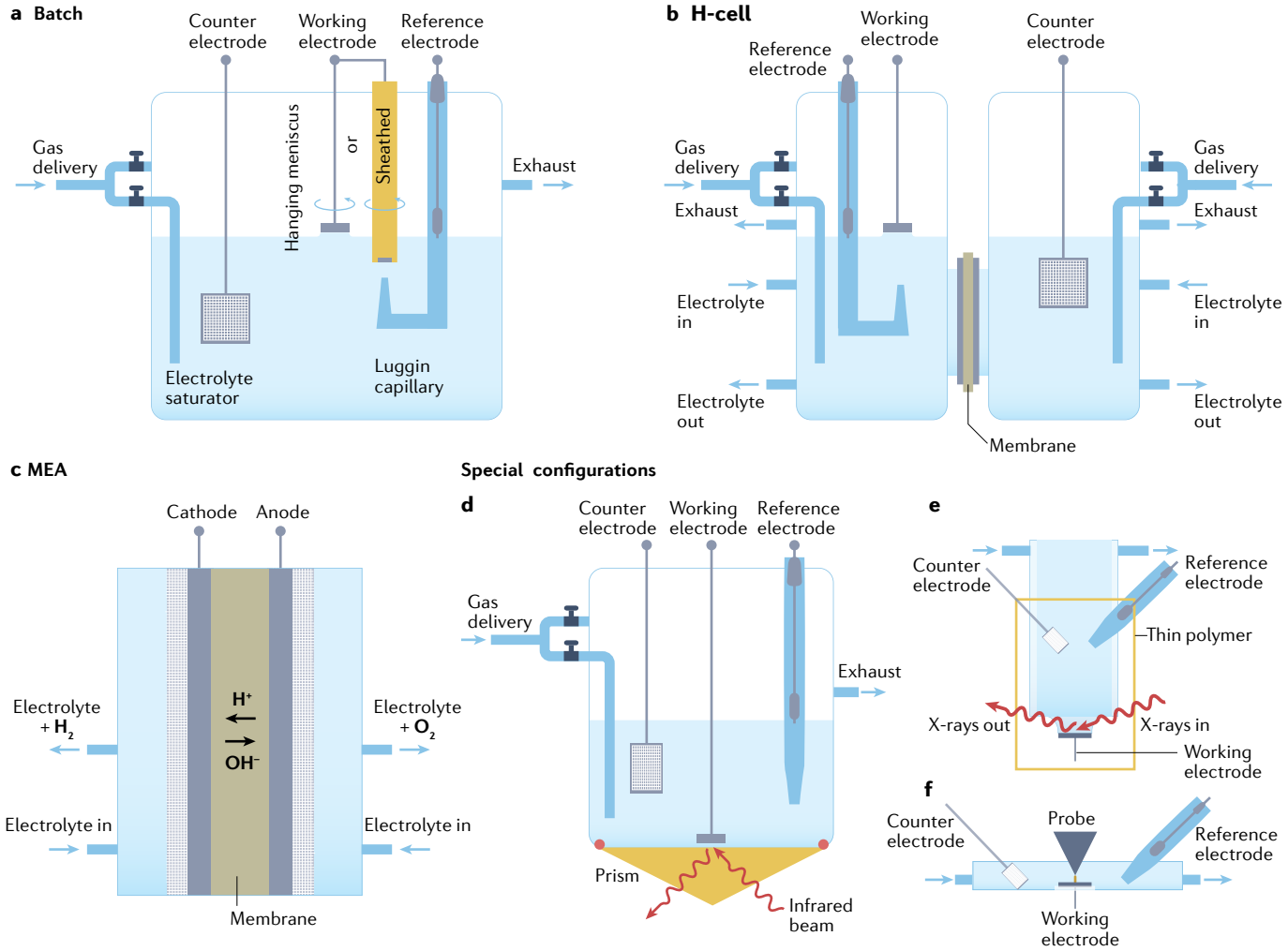


Fig. 2 | **Electrochemical cells. a** | Batch cell. **b** | H-cell. **c** | Membrane electrode assembly cell (MEA). **d** | Special electrochemical cell configuration for in situ infrared spectroscopy. **e** | Special electrochemical cell configuration for surface X-ray diffraction. **f** | Special electrochemical cell configuration for scanning tunnelling microscopy. Individual components are not necessarily to scale.

***Electrolyte.*** The purity of the electrolyte precursors must always be considered, especially in fundamental studies (see Supplementary Table 2). Contamination, particularly anions such as $SO_4^{2-}$, $Cl^-$ and $NO_3^-$, can bind to the surface of the electrocatalysts and block active sites, leading to lower selectivity, lower faradaic efficiencies and impurities in the product. For example, nitrate/nitrite binding on the cathode can lead to nitrate/nitrite reduction[51] and compete with the HER. Contamination by metal ions generally leads to deposition on the surface as metals and metal hydroxides, which can block active sites or promote activity[52,53]; for example, $Fe^{3+}$ impurities in the electrolyte enhance the OER over metal hydroxides and oxyhydroxides[54,55]. Discrepancies in reported oxygen evolution rates over nickel oxyhydroxides were unresolved until iron impurities present in the KOH electrolyte were found to significantly impact the oxygen evolution rate[54].

It is crucial to use sufficiently pure salts and electrolytes, as electrolytes with impurities can significantly impact low current density experiments. For instance, the highest purity caesium perchlorate salts available (99.995%, Sigma Aldrich) were not pure enough for reproducible cyclic voltammograms; multiple recrystallizations of $CsClO_4$ in ultra-high-purity water were required for an electrolyte with reproducible cyclic voltammograms[56]. Similarly, organic ammonium cation-based salts (such as tetrabutylammonium tetrafluoroborate) containing high amounts of impurities can be recrystallized in methanol or ethanol[57]. Cleaning the electrolyte with Chelex (a solid-supported iminodiacetate resin) to remove metal ions has also been reported[58]. $Fe^{3+}$ impurities in KOH have been removed via electrochemical deposition onto Ni–$MoS_2$ electrodes[59] and also captured in precipitated $Ni(OH)_2$ and $Co(OH)_2$ (REF.[54]) followed by filtration of residual metal hydroxide solids[60]. When deuterated water is utilized[61], it should be purified as it often contains metal ion and anion impurities[62] (see Supplementary information Section 1.3).

Accurate quantification of the pH and proton concentration is also of upmost importance. Commercial pH probes have different calibration ranges and at extreme pH can give faulty readings (see Supplementary Fig. 1).

A pH meter that directly measures the hydrogen ion activity is highly recommended (for example, pHydrunio by Gaskatel).

***Contact interface between the working electrode and electrolyte.*** There are two main ways an electrode can contact the electrolyte: embedded within a protective matrix or in a hanging meniscus configuration (FIG. 2a). Enveloping an electrode in an inert polymeric cylinder protects the working electrode's walls from contact with the electrolyte and allows facile collection of currents under hydrodynamic conditions[63,64]. This inert cylinder can be made of polytetrafluoroethylene (Teflon) or other materials such as polyether ether ketone, which is more expensive but exhibits higher rigidity and strength. A second working electrode in the shape of a ring can be added into the cylinder to deconvolute contributions from two parallel reactions, a set-up called the rotating ring disc electrode. The hanging meniscus configuration is ideal for electrodes with varying shapes or sizes, single-crystalline electrodes and when embedding in an inert matrix is not convenient or possible. Here, it has to be assured that only the flat surface and not the edges are in contact with the electrolyte to ensure only the flat surface contributes to the current, not a convolution of both the flat surface and edges[65]. To ensure this, convective dry gas can be flowed over the meniscus to ensure the edges are dry. Electrodes in this configuration can also be used under rotation[65].

***Bubble fouling.*** During water electrolysis at practical reaction rates, gas bubble formation is often unavoidable due to the accumulation of hydrogen and oxygen gas products near the cathode and anode and their limited solubilities in aqueous electrolytes. The life cycle of gas bubbles under this resultant supersaturated condition includes nucleation at the nanoscale, growth, coalescence and detachment from the electrode surface[66,67], as shown schematically in FIG. 3a. The overall gas bubble evolution process influences electrochemical processes and the energy efficiency of water electrolysis in various aspects. For example, blocked active surface area and increased ohmic resistance by insulating gas bubbles result in energy loss. To mitigate this, lower concentrations of dissolved gases (below supersaturation) and induced mass transport — such as through the use of capillary-induced transport[68] — can improve energy efficiency. Details on advancements and understanding on this topic can be found in recent papers[69,70]. Removing macro-sized gas bubbles is challenging, and a few non-exhaustive strategies are presented. Inverted upward-facing working electrodes can facilitate macro-sized gas bubble detachment without accumulation at higher current densities[71,72]. Further, physically dislodging bubbles, for instance with a rod, can improve energy efficiency[73]. Reducing the hydrophobicity of ring disc electrode/rotating ring disc electrode tips by dip-coating in a hydrophilic polymer has also been shown to suppress bubble accumulation[73].

***Gas delivery.*** The gas delivery system in flow cells includes the gas source (such as gas tanks or purification systems for house air), the flow controller (for example, precise mass flow controllers or other less precise flow controllers), any intermediate units (for example, desiccants to capture undesired impurities, bubblers to introduce desired vapours) and the tubing for delivery. As shown in FIG. 2a,b,d, the gas can be bubbled directly through the electrolyte for faster initial saturation and then switched to flow above the liquid to maintain a blanket of gas above the electrolyte. For hanging meniscus set-ups[65], bubbling through the electrolyte often perturbs and breaks the contact between the working electrode and the electrolyte. For sheathed electrodes, gas may be bubbled into the electrolyte during electrochemical measurements to flush away gaseous products. In the case of MEAs, the electrolytes are often pre-saturated prior to flow into the electrolyser.

Gases and gas delivery lines should be contaminant free. Argon and hydrogen with purities of 99.9999% and 99.999%, respectively, result in identical Pt(111) cyclic voltammograms (CVs) in 0.1 M $H_2SO_4$ (REF.[74]) (see Supplementary Table 3). The interior of stainless-steel tubing typically contains organics and particulates and should be cleaned out with alternating washes of acetone and water prior to installation, and in-line particulate filters should be used[75].

***Electrode–electrolyte interface.*** Different factors impacting the electrode–electrolyte interface of a working catalyst are illustrated in FIG. 3. Resistances in the electrochemical system are due to bubbles, charge transfer and solution resistance. Inhomogeneities on the electrode surface can serve as bubble nucleation points. FIGURE 3b highlights how concentration gradients of products, reactants and electrolyte species will always be present to different degrees depending on the conditions of mass transport. These gradients may be minimized by working under severe forced convection or co-feeding products, or maximized by working with porous electrodes[76–78]. Finally, different ionic species will have a different impact on the resistance of the electrolyte solution, on the solution pH and on the electric field near the surface in comparison with the bulk (FIG. 3c).

The factors outlined in FIG. 3 can also influence reaction kinetics. For instance, it has been hypothesized that addition of an anion as a proton acceptor significantly increases

Box 1 | **Contaminants**

**Definition of contaminants**

Contaminants are defined as undesired or unintended species present in an experiment. Almost nothing is ever 100% contaminant free; however, at low enough concentrations, inaccuracies caused by contaminants on macroscopic properties will be much lower than the natural variation from replicates of these macroscopic properties. In electrochemical experiments, these macroscopic properties are typically the cyclic voltammogram, impedance spectra and reaction currents/rates.

**Examples of contamination**

Anything that comes into contact with the electrodes and electrolyte prior to or during electrochemical experiments may introduce potential contamination. The working electrode may be contaminated from precursors or preparation, the counter and reference electrodes or from the electrolyte. The electrolyte may be contaminated from equipment used to prepare and transfer it, ambient air, precursors and stock solutions, cell components, saturation gas or gas lines.

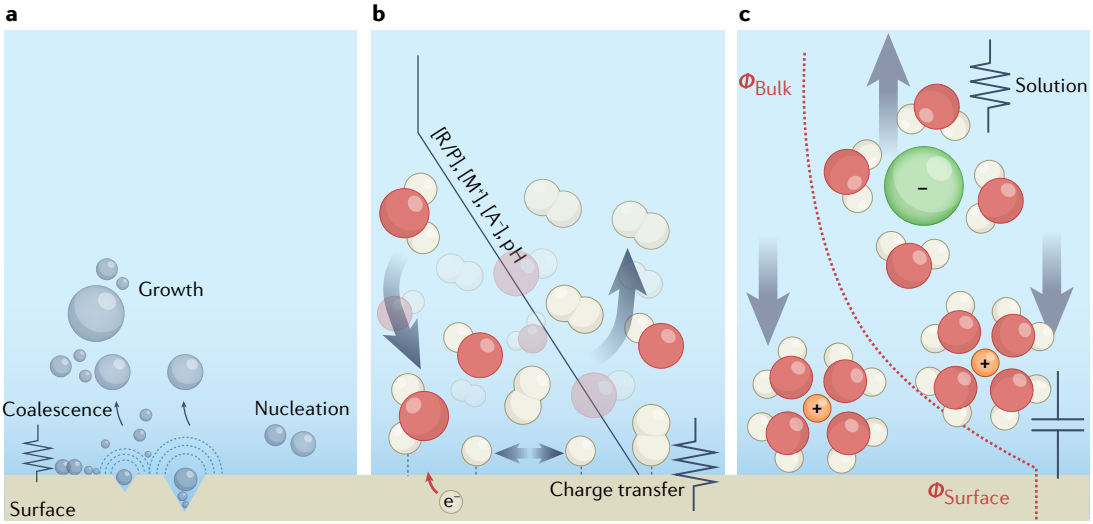


Fig. 3 | **Factors impacting the electrode–electrolyte interface of a working catalyst.** Variables that can affect reproducibility of measured currents are bubble formation, concentration gradients generated by mass transport limitations, system resistances (charge transfer, electrolyte solution), electrolyte ions, migration and convection, among others. **a** | Bubble formation and fouling on the electrode surface. **b** | Concentration gradients generated by mass transport limitations. **c** | Electric field, pH and resistance of the electrolyte solution are impacted by diffusion and migration of ionic species. Schematic depicts the cathode but it should be noted that these factors occur at both the anode and the cathode. $A^-$, anions; $M^+$, cations; P, products; R, reactants.

the water oxidation reaction rate[79–82]. Additionally, confined oxygen bubbles have been shown to shift the OER selectivity towards $H_2O_2$ (REF.[83]).

These remarks are also valid for contaminants, which is why cleanliness is crucial for studying electrocatalytic systems. Finally, to tackle the complexity of the electrochemical environment, systematic characterization and possible corrections are necessary, ideally combining different electrochemical techniques.

### *Characterization methods*

In many cases, measurements of the electrochemical current alone do not suffice to obtain a complete understanding of an electrocatalytic system. Therefore, complementary characterization techniques are used, providing insight into the structure of the electrode[84–95], the nature of the electrode–electrolyte interface[96–116] and the product distribution[117–126] (FIG. 4). Such information indicates what water electrocatalysis looks like on the molecular level, facilitating the interpretation of activity, stability and selectivity trends observed in electrochemical measurements. For example, vibrational spectroscopy has been widely used to identify the coverage and concentration of intermediates. During the HER, for instance, the hydrogen coverage on a platinum electrode could be tracked by infrared spectroscopy[127]. Along the same line, X-ray absorption spectroscopy (XAS)[90,91] is often used to identify the oxidation state and coordination environment of the metal ions in OER catalysts. To understand the selectivity of electrocatalytic systems, product analysis is an essential complement to electrochemical measurements. Using tools such as differential electrochemical mass spectrometry[120–123,128] or a rotating ring disc electrode[73,129,130], one can disentangle water electrocatalysis from competing reactions such as chlorine evolution.

An overview of characterization techniques and general considerations for selecting a suitable technique to study the reactions involved in water electrocatalysis can be found in Supplementary Table 4 and is summarized in FIG. 4. When deciding which characterization technique is best suited for their work, researchers should consider whether the technique can provide the information needed to understand the electrocatalytic system under study and whether the technique is compatible with the electrocatalytic system. Different characterization techniques provide vastly different information, making them suitable for different systems. For example, complex multi-element systems such as alloys, single atom catalysts or (immobilized) metal–organic complexes can benefit from the element-specific nature of X-ray absorption spectroscopy[90,104,108] and X-ray photoelectron spectroscopy (XPS)[90,106,108]. This allows the (chemical) structure of the elements of interest to be probed one at a time, even though they are inside a complex mixture. Other techniques, such as scanning probe microscopy[98,99,115,116] (for example, STM, atomic force microscopy (AFM)) and plasmonically enhanced Raman spectroscopy[96,97,100] (surface-enhanced Raman spectroscopy (SERS) and shell-isolated nanoparticle-enhanced Raman spectroscopy) allow the electrode–electrolyte interface to be probed specifically. This enables the identification of adsorbates and surface structures, even though the electrode–electrolyte interface consists of just a few atomic layers buried between macroscopic amounts of bulk electrode and electrolyte material. Parameters such as sensitivity and time resolution also play an important role. For product analysis, for example, differential electrochemical mass spectrometry[121,122,124,131] is a fast detection method, but it does not have the sensitivity and resolving power of gas chromatography[117,118].

A second aspect that distinguishes the various techniques is the set of restrictions that they impose on the cell, the electrode and the applied conditions. In order to perform in situ characterization inside the fully assembled cell, a specialized geometry is nearly always necessary. For techniques involving light (FIG. 2d), a thin film electrode or a thin electrolyte film between the electrode and a window is used to minimize scattering and absorption[90,91,101]. In the first case, only thin film samples can be used. In the second case, the mass transport around the working electrode may be impeded, making measurements at high current density challenging. Many characterization techniques are not compatible with the bubbles that the HER and the OER generate, making it challenging to study these reactions under true operando conditions (or under kinetic operating conditions in the absence of mass transport effects). Continuous development of improved cell geometries and detection schemes are pushing these boundaries, enabling more true operando measurements and boosting the sensitivity towards the active sites at the electrode–electrolyte interface. Unless the reaction rates and kinetics collected in operando cells match the kinetically controlled rates free of mass transfer, one cannot label their spectroscopic experiments as operando.

Electrochemical characterization in the cell used for operando experiments is also important. Owing to time constraints (at synchrotrons) or the complex cell designs, the standard for clean and reproducible working conditions is not always achieved. It is therefore vital to reproduce the electrochemical data obtained earlier from clean electrochemical cells in the cell used in the synchrotron. Using the OER over NiOOH as an example, if the OER activity increases (up to a factor of 50) with increasing scans, iron impurities are likely to be present in the cell[54]. Damage caused by the beam to the cell parts may also introduce adsorbed contaminants to the surface.

## Results

In this section, important considerations and corrections necessary for analysing and reporting data regarding water electrolysis are discussed. Several earlier indispensable contributions also cover the reproducible analysis and reporting of electrochemical results[14,132–137].

### *Intrinsic currents*

To ensure reported currents are reproducible and not convoluted, several corrections and tests must be performed. Internal resistance through the electrolyte between the working and counter electrodes must be measured (often with impedance spectroscopy) and corrected by 100%. Real-time correction by 100% can lead to unstable feedback loops[138]. To ensure stability, 85% of the internal resistance can be corrected during data collection and then the additional 15% corrected during post-analysis, or data can be collected with no internal resistance correction and then corrected 100% during post-analysis. External transport limitations in the bulk electrolyte from the reaction-consuming reactant

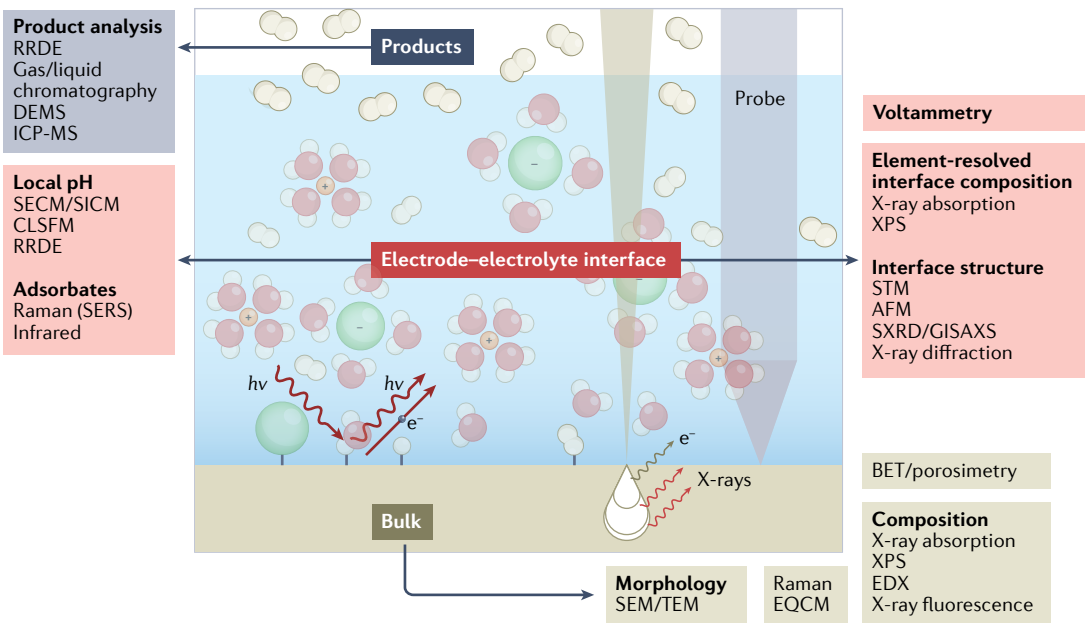


Fig. 4 | **Overview of important complementary characterization techniques in electrocatalysis.** A plethora of characterization techniques enable us to probe products, the electrode–electrolyte interface and the bulk electrolyte. AFM, atomic force microscopy; BET, Brunauer–Emmett–Teller; CLFSM, confocal laser scanning fluorescence microscopy; DEMS, differential electrochemical mass spectrometry; EDX, energy dispersive X-ray spectroscopy; EQCM, electrochemical quartz crystal microbalance; GISAXS, grazing-incidence small-angle X-ray scattering; ICP-MS, inductively coupled plasma mass spectrometry; RRDE, rotating ring disc electrode; SECM, scanning electrochemical microscopy; SEM, scanning electron microscopy; SERS, surface-enhanced Raman spectroscopy; SICM, scanning ion conductance microscopy; STM, scanning tunnelling microscopy; SXRD, surface X-ray diffraction; TEM, transmission electron microscopy; XPS, X-ray photoelectron spectroscopy.

Table 1 | **Properties that can be used for rate normalization, increasing complexity**

| Property for normalization | Advantages | Disadvantages | Determination |
|---|---|---|---|
| Geometric area ($mA\,cm_{geometric}^{-2}$) | Useful quantity for industry, reproducible quantity for single crystal surfaces | Overestimates rates on materials with high density of active sites or high surface area | Geometric area of the electrode |
| Mass ($mA\,g^{-1}$) | Useful quantity for industry (cost analysis), reproducible quantity for single crystal particles with same particle size distribution | Often underestimates rates on materials where the bulk does not contribute to the catalysis | Mass deposited<br>Elemental analysis techniques such as inductively coupled plasma, XPS and so on |
| Surface area ($mA\,cm_{SA}^{-2}$) | Good for comparing electrodes with drastically different surface areas | Can overestimate rates by over-counting active surface area/sites[152] | Via selective interaction with probe molecules, for example integral of regions in CVs such as $H_{UPD}$ and CO stripping; BET surface area; surface redox reactions, pseudo-capacitive region[280], microscopy |
| Active sites ($mol_{product}\,mol_{active\,sites}^{-1}\,s^{-1}$) | Gives most insight into the nature and identity of the active site(s) | Challenging and requires kinetic verification via TORs and correlations | Same as above |

BET, Brunauer–Emmett–Teller; CV, cyclic voltammogram; $H_{UPD}$, hydrogen underpotential deposition; TOR, turnover rate; XPS, X-ray photoelectron spectroscopy.

should also be corrected for. This involves, for example, measuring the current at different rotation rates and extrapolating to an infinite rotation rate using the Levich equation[133,139]. For porous electrodes, the Thiele modulus and effectiveness factor can also be calculated to determine whether transport within channels and pores (which are not influenced by bulk external convection induced by rotation) may be rate limiting[76,140]. At large overpotentials, reactions are no longer kinetically limited but, rather, limited by bubbles and/or mass transport towards and away from the electrocatalytic interface. Under these sluggish mass transport conditions, the pH near the surface can differ significantly from the bulk pH of the electrolyte even if a buffer solution is employed[141]. Determining the value of the local pH can help separate its effect from other variables that may influence the reaction[130,142–144], and nowadays several techniques are available for performing such measurements[142].

### *Turnover rates and rate normalization*

The most rigorous way to report reaction rates is to normalize intrinsic currents to the number of active sites, a quantity called the turnover rate (TOR) or turnover frequency[135,145–147] (Eq. 6). If active sites are single-site and properly quantified, then the TOR should be constant at a given potential (for example, metal loading):

$$\mathrm{TOR} = \frac{\text{Reaction rate}}{\text{Number of active sites}}\,[=]\,\frac{\mathrm{mol}_{\mathrm{product}}\,\mathrm{s}^{-1}}{\mathrm{mol}_{\mathrm{active\ sites}}} \tag{6}$$

Identifying and quantifying the number of active sites can be challenging. Each catalytic system is unique and requires creativity and rationality in both the identification and quantification of active centres[148]. Because it is challenging to identify and count active sites, other properties are often used to normalize reaction rates, as summarized in TABLE 1.

Normalizing to the geometric area is a useful quantity for industry as space is an important criterion in scaling up. Unless the electode is truly flat, such as single crystal surfaces[149], normalizing to the geometric area often leads to inflated rates. Reaction rates per catalyst mass are also important due to cost implications. Unless the catalyst contains single-site active centres, normalizing to the catalyst mass often deflates the rates because of dispersion: only the portion of the catalyst surface in contact with the reactants can directly contribute to the reaction[150].

The surface area can be quantified using various techniques, often by counting the number of probe molecules that can blanket the electrode (such as Brunauer–Emmett–Teller (BET) $N_2$ adsorption or chemisorption) or using microscopy. When the adsorption, desorption or reaction of probe molecules is controlled electrochemically, this surface area quantity is often referred to as the electrochemical surface area[151]. These electrochemical methods may undercount the true electrochemical surface area, leading to inflations in the normalized rates[152].

Experiments should be designed to rigorously quantify active sites, resulting in a constant TOR independent of the active site density[153]. Convincing evidence often involves a linear correlation between intrinsic currents and the number of active sites or area. For example, a linear relation was observed between the HER rate and the length of $MoS_2$ edge sites[154]. Another study observed a correlation between OER rates and the number of nickel atoms able to oxidize to NiOOH at approximately $1.35\,V_{RHE}$ and demonstrated that the TOR is independent between nickel loadings of 0.2 and $0.4\,mg\,cm_{geometric}^{-2}$ (REF.[155]). At nickel loadings above $0.4\,mg\,cm_{geometric}^{-2}$, OER rates were lower than predicted from a linear extrapolation — a strong indication of mass transfer limitations[155]. Similarly, it was observed that OER rates correlated with the number of unsaturated sites on $IrO_2$ and $RuO_2$ catalysts[156]. It has also been claimed that OER active sites exhibit different properties from the inactive material, as measured using electrochemical impedance spectroscopy and electrochemical STM[157–160].

Utilizing the TOR is easiest when there is only one dominant active site. However, in the case where a distribution of active sites each with different reactivity exists, a linear combination of all significant entities would be an appropriate approach. For example, scanning electrochemical cell microscopy can quantify OER activities on

Thiele modulus
The ratio of the reaction rate to the diffusion rate.

Effectiveness factor
The ratio of the experimentally measured reaction rate to the kinetic reaction rate in the absence of diffusion limitations.

Tafel slopes
The required increase in potential to increase the reaction rate by ten times.

different $CoO_x$ facets, enabling the deconvolution of the overall reaction rate into individual TORs[161].

### *Reaction kinetics*

Reaction kinetics (Tafel slopes, reaction orders and activation energies) can aid in understanding how parameters affect the reaction rate and in identifying reaction mechanisms. These parameters can be calculated by the slope of linearized rate expressions (Eqs. 7–9):

$$\text{Tafel slope} = \frac{\mathrm{d}(E)}{\mathrm{d}(\log(j))} \tag{7}$$

$$[\text{Species}]\text{order} = \frac{\mathrm{d}(\log(j))}{\mathrm{d}(\log[\text{Species}])} \tag{8}$$

$$E_{\text{app}} = -R\frac{\mathrm{d}(\ln(j))}{\mathrm{d}\left(\frac{1}{T}\right)} \tag{9}$$

where $E$ is the potential (V), $j$ is the current density ($A\,cm^{-2}$), [Species] is the concentration of a species in the electrochemical environment, $E_{app}$ is the apparent activation energy ($kJ\,mol^{-1}$), $T$ is the temperature (K) and $R$ is the gas constant.

Proposed catalytic reaction mechanisms can be broken up into a series of elementary steps where the rate of the slowest step (rate-limiting step) is equal to the overall reaction rate[17,140]. Reaction orders indicate how species inhibit or promote the overall reaction rate. Kinetic parameters can be predicted by solving for rate laws, or more rigorously analysed with microkinetic modelling to include fractional surface coverages[162–164]. For the HER, although one can determine the rate-limiting step if the Tafel slope is $30\,mV\,dec^{-1}$ (Tafel rate-limiting step) or $40\,mV\,dec^{-1}$ (Heyrovský rate-limiting step) a Tafel slope of $120\,mV\,dec^{-1}$ alone is unable to distinguish between the Volmer or high overpotential (high coverages) Heyrovský step as rate limiting. In the OER, however, different combinations of rate-limiting steps and surface coverages can exhibit the same Tafel slope, meaning the rate-limiting step cannot be determined solely from Tafel slopes[162]. Additional characterization is required to further determine plausible rate-limiting step(s). Tafel slopes and reaction orders often change dynamically with potential and so the Tafel slope should be reported as a function of potential for ease of comparison and benchmarking between studies, such as to make Tafel slope plots[165]. When linking Tafel slopes to a fundamental rate-limiting step, it is essential that the system operates in the kinetic regime, free of mass transport effects[76,77,166]. At higher current densities, mass transport and bubble formation issues can drastically impact kinetic parameters, and will lead to an apparently increasing Tafel slope if mass transport is not corrected for. Kinetics also must be analysed in a potential regime where the backward reaction is negligible — away from equilibrium. For the HER, one must report kinetics sufficiently away from equilibrium (0 V versus RHE at 298 K) (see Supplementary information Section 1.7). This is not an issue for the OER because measurable currents often occur at large overpotentials sufficiently far from equilibrium (1.23 V versus RHE at 298 K).

As an example, FIG. 5 presents fundamental work in which the HER is investigated on a stationary polycrystalline platinum electrode in LiOH and KOH electrolytes[167]. A blank cyclic voltammogram of the platinum electrode is recorded in argon-saturated 0.1 M $H_2SO_4$ at $50\,mV\,s^{-1}$ prior to every set of measurements (FIG. 5a). The electrochemically active surface area of the platinum is calculated by integrating the hydrogen desorption region between 0.06 and 0.60 V versus RHE (after subtraction of the double-layer charge), considering a surface charge density of $230\,\mu C\,cm^{-2}$ reported for a polycrystalline platinum surface in sulfuric acid[168]. Prior to measurements, for each different electrolyte or concentration, impedance spectroscopy is performed to determine electrolyte resistance and the potential is thus corrected. A cyclic voltammogram of different electrolytes (0.1 M LiOH or KOH) is recorded (FIG. 5b) and the corresponding Tafel plot displayed (FIG. 5c) for the relevant potential range. It is important to calculate the Tafel slope in the kinetic regime to avoid the convolution of hindered mass transport, and also in the regime where the backward hydrogen oxidation reaction is negligible. Here, for example, in LiOH a Tafel slope of $50\,mV\,dec^{-1}$ is found, indicating the Heyrovský step as rate limiting. In KOH a much larger Tafel slope is observed, suggesting a change in the reaction mechanism in which the Volmer step becomes rate limiting. The Tafel slope plot (FIG. 5d) exhibits slopes of approximately 50 and $100\,mV\,dec^{-1}$ for LiOH and KOH, respectively; the sudden increase in Tafel slopes at more negative potentials is due to the onset of mass transport limitations and is proportional to the increase in current density. Next, the effect of the concentration of $K^+$ on the HER in alkaline media is studied by recording cyclic voltammograms in 0.01 M KOH (pH 12) with different concentrations of $KClO_4$ added to the electrolyte (FIG. 5e). This was done using a platinum rotating disc electrode to minimize the effect of hindered mass transport. FIGURE 5f plots the correspondent reaction orders on the $K^+$ concentration at different potentials. Based on the negative slope, it can be concluded that under these reaction conditions, increasing the $K^+$ concentration is detrimental to HER activity.

The effect of temperature can also be used to gain both kinetic[169–173] and thermodynamic[174–176] insights into the electrochemical reaction studied. From the temperature dependence of the reaction rate, both the apparent activation energy and the pre-exponential factor[177] can be determined according to the Arrhenius equation. To compare apparent activation energies between different experimental conditions and with density functional theory (DFT) simulations, it is recommended to use the exchange current density as this gives an activation energy independent of potential[178]. Extrapolating to the equilibrium potential to obtain the exchange current density is often inaccurate because one extrapolates (far) outside the range of measurements. Therefore, it is more desirable to measure at fixed overpotential, but for this knowledge of how the (standard) equilibrium potential changes with temperature is required.

At any other potential, there is a potential-dependent component in the activation energy according to Eq. 10,

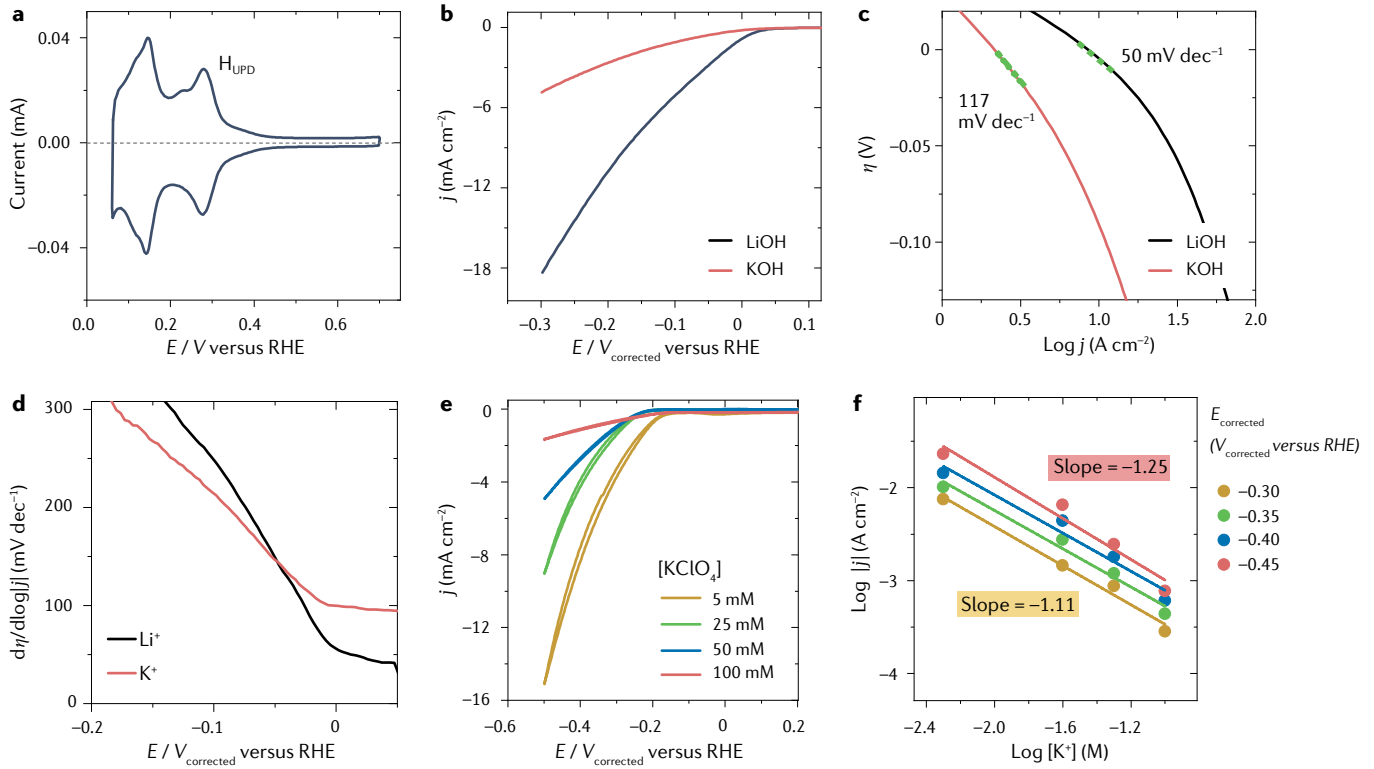


Fig. 5 | **Example of data work-up for the study of hydrogen evolution on a polycrystalline platinum electrode. a** | Blank voltammetry of the platinum electrode recorded in 0.1 M $H_2SO_4$ at 50 mV $s^{-1}$ used for calculating the surface area. **b** | Voltammetry of the hydrogen evolution reaction in 0.1 M LiOH and 0.1 M CsOH recorded at 50 mV $s^{-1}$. **c** | Correspondent Tafel plot. **d** | Tafel slope plot. The increasing Tafel slope at more negative potentials is due to mass transfer limitations. Cation concentration-dependence study recorded on a platinum rotating disc electrode at 2,500 rpm. **e** | Voltammetry in 0.01 M KOH (pH 12) with different concentrations of $KClO_4$ added to the electrolyte. **f** | Correspondent reaction orders on the $K^+$ concentration at different potentials. The potentials in panels **b**–**f** have been corrected for the solution resistance, which was measured via impedance spectroscopy. RHE, reversible hydrogen electrode. Adapted with permission from REF.[167], ACS. $H_{UPD}$, hydrogen underpotential deposition.

where $\Delta H_c^{\ddagger}$ is the activation enthalpy, $\alpha_H$ is the enthalpic transfer coefficient, $F$ is Faraday's constant and $\eta$ is the overpotential:

$$\Delta H_c^{\ddagger} = \Delta H_{0c}^{\ddagger} + \alpha_H F \eta \tag{10}$$

Another kinetic parameter that can be determined with temperature experiments is the transfer coefficient, which consists of an enthalpic and an entropic component[179,180]:

$$\alpha = \alpha_H + T\alpha_s \tag{11}$$

The enthalpic component can be determined using Eq. 10 whereas the entropic component can be determined by plotting the natural logarithm (ln) of the pre-exponential factor versus temperature. A second way to determine both parameters is by using the Tafel slope at different temperatures[170] (Eq. 12), where $b$ is the Tafel slope and $\alpha_s$ and $\alpha_H$ is the entropic and enthalpic transfer coefficient, respectively:

$$\frac{1}{b} = -\frac{\alpha_s F}{2.303R} - \frac{\alpha_H F}{2.303R}\frac{1}{T} \tag{12}$$

For accurate determination of these kinetic parameters, it is important to consider some aspects that are unique to electrochemical experiments at temperatures other than room temperature. These experiments can be carried out in two ways[181,182]: either in an isothermal cell with the reference electrode at the same temperature as the working electrode, or in a non-isothermal cell where the working electrode compartment changes temperature while the reference electrode compartment is maintained at 25 °C. In the isothermal cell, the temperature-induced change of the equilibrium potential of the reference electrode is considered both explicitly in the Nernst equation and through the temperature dependency of the standard equilibrium potential and the activity of the ions[183]. For HER studies, the RHE is recommended for isothermal cells as there is no need to consider shifts in the equilibrium potential. For the OER, knowledge of how the OER equilibrium potential changes on the temperature-dependent RHE scale is required, which is not so trivial. In the non-isothermal cell, the potential of the reference electrode is stable, but there exists a thermal junction potential difference between the reference electrode and the working electrode, which is unknown if not measured for the specific electrolyte used[182].

Other factors should be considered and potentially corrected for when experimentally measuring apparent reaction orders, Tafel slopes and apparent activation energies. The solubility of gases changes with pressure and temperature; in aqueous solutions, the solubility of gases can be calculated using Henry's law correcting for the equilibrium constants using the van't Hoff

equation or with empirical data[184]. This is much more of a challenge for Tafel slopes as electrochemical bias induces local gradients between the bulk and the surface. Correcting for solubility effects enables a comparison of currents under the same local conditions. Second, the standard equilibrium potential also changes with temperature, meaning that the same applied potential does not result in the same overpotential; this change can be calculated using thermodynamics. It has been demonstrated that failing to correct for thermodynamic changes in the solubility can lead to incorrect reaction orders and, thus, interpretations of the HER mechanism[185]. Comparing currents and kinetic parameters between the RHE (where the reference electrode shifts with the pH) and the normal hydrogen electrode scale (pH-independent) can be used to determine whether the HER rate-limiting step involves protons or hydroxides[143]. Additionally, kinetic isotope effects can complement Tafel slopes and reaction orders to give insight into mechanistic details of rate-limiting steps[186–188].

### *Theory considerations*

Complementary to experimental analysis of reaction thermodynamics and kinetics, and the identification of reaction intermediates and products via characterization, is the use of DFT computational modelling. Under specific assumptions, DFT offers atomic-scale insights into the thermodynamics and kinetics of reactions[189–191], vibrational frequencies of different adsorbates[96,192], the effect of a homogeneous electric field within the electrical double layer[193], the role of applied electric potential and bulk pH[194], adsorbate coverages[190], catalyst oxidation states[195–197] and the role of electrolyte species[198,199] (see FIG. 6). On the other hand, systematic assessment of mass transfer phenomena, including surface pH effects, and potential-driven surface reconstruction requires multiscale approaches, which are at the boundaries of the current capability of DFT simulations[200–202].

The typical protocol for modelling the HER and OER consists of two steps. First, it implies the definition of simplified models with reaction intermediates adsorbed on a few atomic layers representative of surfaces. Later, formation energies for these adsorbates are estimated from their binding energy. Formation energies of intermediates characterized by analogous bond order with the catalytic surface correlate among themselves, giving rise to thermodynamic linear scaling relationships[203] that, as in the case of the OER, may intrinsically limit the reaction activity[204,205]. The effect of the applied electric potential and bulk pH in the reaction thermodynamics is included in DFT via the computational hydrogen electrode scheme[194], which implies a shift of the Gibbs free energy of a reaction step by a term dependent on the potential (versus RHE) and the number of concerted proton-coupled electron steps until that reaction stage (see Supplementary Eq. 8). As activation energies correlate with formation energies of intermediates according to the Brönsted–Evans–Polanyi relation[206–208], thermodynamic properties can provide insights into the reaction kinetics as well. Thus, this framework enables the definition of thermodynamic or kinetic descriptors for the activity of the HER and OER.

Correlation between descriptors and reaction activity is typically represented through a volcano relationship between the experimental current density observed experimentally and intermediates binding energies computed through DFT[189,190,209]. Although this modelling protocol has proved effective in determining the most active HER and OER catalysts, further parameters must be assessed to model the overall system. For example, considering the HER in neutral to alkaline bulk pH, the OH binding energy and the activation energy for water dissociation are relevant thermodynamic and kinetic descriptors[190,199,210] (see Supplementary Eq. 8). Still, electrolyte species, as cations, may facilitate or hinder the HER depending on the pH regime, catalyst and orientation of solvation molecules[96,167,190,199], and thus they should also be included within the simulation cell (see Supplementary information Section 3). In the case of the OER, computationally derived Pourbaix diagrams allow one to identify materials which are thermodynamically stable within a specific bulk pH and electric potential regime, thus extending modelling predictions beyond just the catalyst activity[211–214].

Recently, additional methods to assess the effect of electric potential in reaction kinetics have been developed, such as grand-canonical DFT[215]. Differently from the computational hydrogen electrode scheme, in a grand-canonical DFT simulation the number of electrons in the system varies to keep their electrochemical potential constant[216]. By changing the number of electrons, it is possible to tune the electrode potential[217]. As DFT simulation cells must be neutral, such additional electrons should be compensated for — for example, by a uniform positive background across the system, as in the solvated jellium method[215]. Additional insights into the methodology and application of grand-canonical DFT can be found elsewhere[217–219].

## Applications

In this section, practices relevant to applied research in electrochemistry are described, focusing on water electrolysis. Specifically, we discuss considerations that need to be taken into account in environments such as a company's research and development department seeking to move a process from the laboratory into the commercial world[220].

### *Laboratory-scale applied research*

In applied water splitting studies, research should focus on minimizing costs and, in the case of a large-scale electrochemical process, maximizing production (within the market limits). This roughly translates to maximizing the current density and the current efficiency while minimizing the cell voltage and operating the cell for as long as possible without interruptions. It is also imperative to consider the process as a whole, including the separation of the final products and waste handling, which may cause the cell to run in suboptimal conditions if an advantage is created downstream in the process.

### *Catalyst considerations*

The core of the electrochemical cell is the catalyst. First, whether the catalyst is active and selective under industrial conditions should be considered; a promising

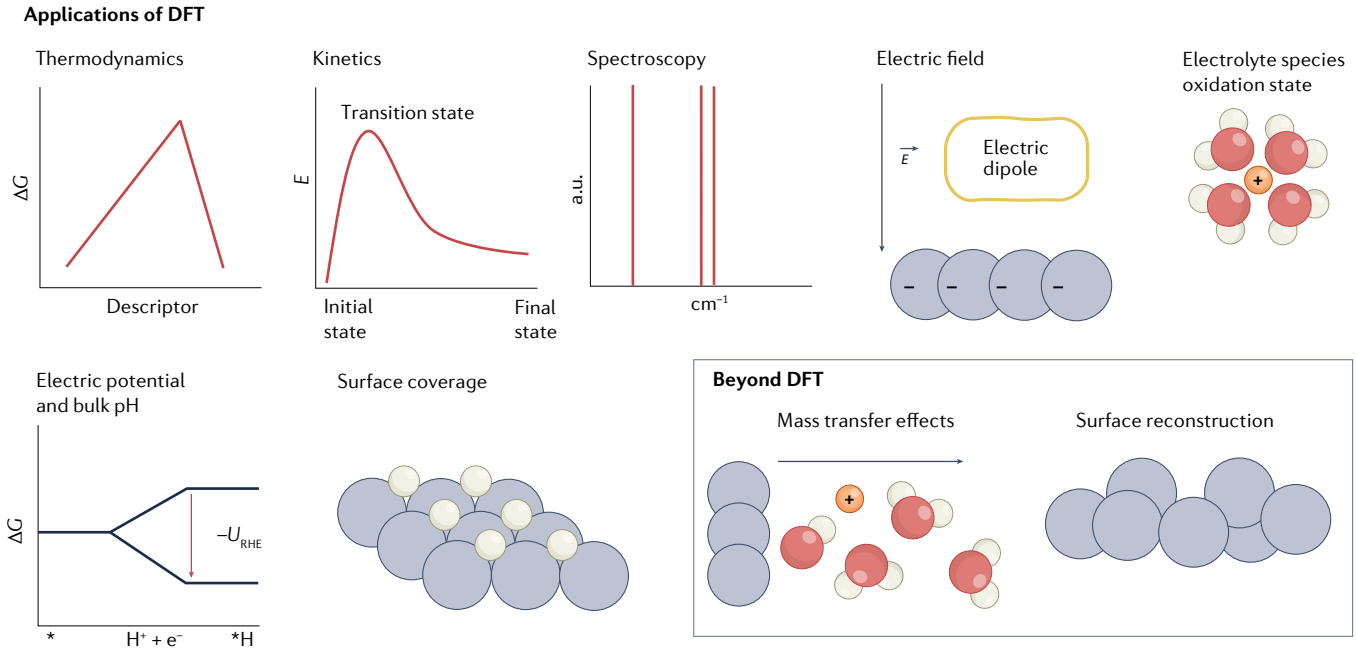


Fig. 6 | **Density functional theory modelling for water electrolysis.** Applications and limitations of state-of-the-art density functional theory (DFT) modelling for water electrolysis. RHE, reversible hydrogen electrode.

catalyst in optimal conditions may not perform well in real conditions. Another consideration is whether the catalyst can be synthesized to achieve a high surface area and be incorporated as an electrode; it might not be straightforward to retain the features that make a certain bulk electrocatalyst active when produced in the form of nanoparticles. Whether the electrode is physically stable, corrosion-resistant and active for long periods of time also need to be considered because catalyst stability is very often a significant challenge. Although HER currents in acidic environments are two to three orders of magnitude higher than in a basic environment[221], the most well-established water electrolysis process is alkaline water electrolysis. This is primarily because of severe corrosion issues in using acidic electrolytes. Metals in alkaline environments tend to passivate and be somewhat protected from corrosion. In addition, nickel-based catalysts are suitable as electrode materials for alkaline electrolysis, greatly decreasing the capital costs deriving from the use of platinum group metals in acidic electrolyte. Typical concentrations of the NaOH or KOH solutions used in these cells range from 25–30 wt% up to 40 wt%, and the cell is operated at temperatures up to 120 °C (REF.[222]). These are harsh conditions, and the materials employed in the electrochemical cells need to withstand them.

### *Commercial electrochemical cell design*

Commercial cells for testing are seldom found at scales larger than 10 $cm^2$. Therefore, customizing a cell for the desired testing size may be necessary. The materials of the cell and testing apparatus need to be compatible with the electrolytes used and at the operating temperatures. The gap between the electrodes, the flow distribution inside the cell and the seal between the compartments and the membrane should be considered when designing a cell. The gap between electrodes directly affects the cell voltage. Additionally, with an increase in cell size, high cell voltages lead to larger heat generation resulting in higher temperature electrolytes. This can appear to be beneficial as the cell potential decreases with higher operating temperatures, and the heat generation could be used to maintain the high operating temperature of the cell. However, minimizing the energy consumption of the cell (through reducing the cell potential and maximizing the current efficiency) is a greater priority[223].

The flow distribution in the cell needs to ensure a uniform velocity of electrolyte through the cell so that there are no dead zones that can affect the mass transfer and the current distribution across the electrode. Additionally, for alkaline water electrolysers, the flow distribution on the cell outlet needs to allow any gas bubbles to escape and not accumulate inside the cell's active area. Gas accumulation inside the cell leads to a reduction in the cell active area and an increase in cell voltage[224,225]. The understanding of gas bubble evolution inside the cell is beneficial to cell and electrode design to further optimize the energy efficiency of the system. The flow distribution especially becomes necessary to consider when experimenting with cell stacks (multiple cells combined into one unit). Ensuring uniform flow and current distribution to all cells in a stack is important. COMSOL is a computational fluid dynamic simulator and multiphysics solver that can be used to examine the flow, gas generation and current distributions in cell designs before fabrication and physical testing[226].

### *Operating conditions*

The whole electrochemical cell should be considered when investigating a specific process, and the decrease in cell voltage needs to be achieved by optimizing both the cathodic and anodic compartments. It is possible that in an electrochemical cell, two different electrolytes

are used for the anodic and cathodic compartments and that an appropriate membrane or separator needs to be chosen. For example, using a dilute base as an anolyte for oxygen evolution and separating the cell with a cation exchange membrane can lead to the depletion of the anolyte and a progressive increase in cell voltage in the case of a batch system. Moreover, a poorly designed electrochemical cell or the use of dilute electrolytes can impact the cell voltage, much more than the overpotentials of the electrochemical reactions. For this reason, the use of concentrated, conductive electrolytes is warranted. These aggressive electrolytes can speed up catalyst degradation or change its reactivity, leading to discrepancies between the laboratory bench and real devices[227]. Therefore, it is important to test the materials in realistic environments (for example, with MEAs) from the very beginning of the catalyst-discovery process[228,229].

An important difference between fundamental and applied research is the focus on potentiostatic versus galvanostatic methods. The control of the potential of an electrode is a complex endeavour in electrochemical cells at high currents. Even with highly conductive electrolytes, the high currents cause substantial ohmic drops. Additionally, the evolution of gases, the changes in temperature from heat generation and the formation of concentration gradients in the cell complicate the situation. Moreover, the large electrodes employed will not have a homogeneous potential distribution on their surfaces. For these reasons, the experiments are usually performed with a power supply, and constant currents are applied to the cells.

### *Hydrogen purity considerations*

The requirements for the purity of hydrogen produced from electrolysis will vary based on the end use of the hydrogen. Hydrogenation processes can utilize a hydrogen gas feed with a purity of 98% whereas fuel cells require hydrogen purity to be more than 98.98%[230,231]. Standards for hydrogen purity requirements are set in ISO Standard No. 14687:2019. Oxygen from cross-over through the membrane and water are two of the main impurities in hydrogen produced from electrolysis[232]. The reduction in the concentration of these impurities in the product stream and the downstream separations of these impurities should also be considered in future research. Specifically, membranes can be developed, modified and tested to reduce the amount of oxygen cross-over in the electrolysers[231].

## Reproducibility and data deposition

### *Factors affecting reproducibility*

The ability to reproduce results and fairly compare performances is of critical importance to advance in the field. A large number of papers have advocated for standards and protocols to improve electrochemical comparisons between the countless formulations synthesized and tested[16,123,134,135,152,233–240]. Minimum reporting standards include the elemental composition, the cyclic voltammogram, the kinetic catalytic activity (collected under both linear sweep voltammetry and steady-state conditions[241]) normalized to the geometric surface area, the electrochemically active surface area and the mass of the catalyst. Confirmation of the lack of mass transport limitations (rotating for external mass transport, and varying the catalyst loading to probe internal mass transport) is also recommended in addition to a measure of stability such as cycling between relevant potentials and/or holding at industrially relevant currents (typically at 10 mA $cm^{-2}$ for the OER[236]) or potential for an extended time. Reference catalysts such as commercial platinum/carbon[134,242] for the HER and $RuO_2$ and/or $IrO_2$ (REF.[243]) for the OER can be purchased or synthesized. Results should be collected and reported in triplicate (or more) with explicitly defined error bars. If repeats are challenging or time consuming, utilizing error propagation[244] to estimate errors is an alternative. Error bars can be used to determine whether changes in a particular variable of interest (for example, impurity concentration,) significantly impact performance metrics[245].

Owing to the ease of collecting and plotting polarization curves (current versus potential graphs), a plethora of papers exist in the literature where these polarization curves are presented but report kinetic parameters at conditions that are not directly comparable. This presents opportunities to extract[246–248] rate information and compare results on a fair basis; it was recently demonstrated that, for the last two decades, only minimal improvements in the intrinsic activity of catalysts have occurred[249]. Data extraction tools used to mine old literature, data sharing using databases (for example, Catalysis-Hub[250], ioChem-BD[251] and CatApp[252]) and data repositories for both experimental and computational data are strategies and pathways to accelerate impact and progress in catalysis science. In fact, adequate protocols for data collection, cleaning and curation will be crucial to enable quick high-throughput screening of stored data sets through machine learning[253], as already demonstrated for optimization of membranes and material discovery[254,255].

## Limitations and optimizations

The impact of incidental contamination can influence electrochemistry; the benchmarking and comparison of CVs, reaction rates and kinetic parameters in the literature, if available, is encouraged. The process to properly clean, set up and validate an electrochemical cell can be lengthy, but has major future benefits for technological progress. Naturally, optimization of the experimental workflow comes with experience. For instance, once cells are initially cleaned and used, they can often be re-cleaned by boiling several times in ultra-high-purity water without the need to undergo the time-intensive acid wash (see Supplementary information Section 1.1 and Supplementary Table 1). Eventually, these cells will become contaminated, presumably from contaminants from the ambient air and surfaces, so that the CVs, reaction rates and kinetic parameters are no longer reproducible.

When coupling aqueous electrochemistry with characterization techniques, challenges arise from combining the components of a typical electrochemical cell with the characterization technique in question. Spectroscopic techniques are constrained to potential ranges free from bubble formation as bubbles interfere with the photon beam. For intense photon beams such

as those from synchrotrons, one must be wary of beam damage to the working electrode (possible alterations of the surface morphology, composition), to the electrolyte (radical formation, decomposition) and even to the cell, depending on the material[256]. Lastly, limitations inherent to the characterization equipment itself (for example, from gas chromatograph sampling) can also direct how experiments are designed.

One of the biggest challenges in modelling electrochemistry is identifying key factors that affect electrocatalytic performance. Less crucial factors can be disregarded in the model, leading to feasible simulation times. Depending on the experimental study, computational models of electrocatalytic interfaces may be limited to simplified surfaces, low coverage adsorbates and solvation, or include other electrolyte species (cations, anions), electric fields and coverage effects. The choice of set-up should aim at the best agreement with experimental benchmarks. As experimental systems often involve a complexity far beyond the limited power of the current supercomputers, selected experiments with a fixed degree of variables should be performed to validate or falsify theoretical predictions. Insights from validated models can then trigger future experimental studies in the framework of a joint effort towards mutual improvement[257]. Cross-checks between theoretical/computational predictions and experiments are crucially important, also to avoid confirmation bias.

## Outlook

With the impacts of climate change becoming more apparent, there is ever-growing pressure to quickly shift from our current unsustainable linear economy that relies on fossil fuels to a sustainable circular economy. In this section, we provide an outlook on catalyst considerations for scaling up water electrolysis and revisit the role of hydrogen in a sustainable circular economy.

### *Large-scale water electrocatalysis*

***Catalyst considerations for scale-up.*** The production of catalysts by chemical reduction can be hampered industrially by numerous factors. For example, large-scale water electrocatalysis requires large reactors to transport high volumes of liquid, often dangerous and polluting organic solvents. The fast addition of reagents may be difficult on a large scale due to difficulties in the mixing of fluids and the use of expensive, unavailable or toxic reagents[258]. These problems can make it challenging to adopt a catalyst for a large-scale industrial process. An outstanding catalyst made of elements that are too expensive or rare, or that is only obtainable with an elaborate synthesis, could be easily supplanted by a more available lower-performing one.

Another critical point is the catalyst's resistance and response to impurities. Although it is vital to investigate catalysts in ultra-clean systems at the fundamental level, cleanliness comes at a cost. A rugged catalyst able to operate in various conditions could be preferred over a more active catalyst needing an environment that is more costly to sustain at a large scale[259]. DFT can be used to screen potential poisons that may be found in actual stream feeds[260,261]. Once clean and reproducible baseline electrochemical systems have been established, the impact of potential impurities should systematically be studied.

The choice of an anodic reaction alternative to the OER can also provide an additional revenue stream to the overall process and, potentially, reduce the cell voltage. The production of chlorine at the anode, using the anode for electrochemical wastewater treatment or performing another oxidation reaction could be beneficial for the economics of the entire process. Running a reaction other than the OER at the anode could also be more thermodynamically favourable and result in a reduction in the cell voltage[262–264]. Additionally, the cell voltage could benefit from the alternative reaction if there is no gas evolution or bubble formation at the anode. This idea of hybrid water electrolysis has been discussed, but currently there is limited research published on experimental work in this area[265–267].

***Stability and prolonged runs.*** The main focus of laboratory-scale industrial catalyst research for production purposes should be to find clean, scalable and cheap synthesis methods for promising catalytic materials and to investigate the long-term stability and performance of electrodes fabricated with these catalysts in real conditions and high currents[123,268–274]. An important point is the time scale of catalyst stability for industrial application. Industrial electrolysers have lifetimes in the order of several tens of thousands of hours[222]. This makes the assessment of the viability of new catalysts extremely challenging and calls for the development and application of accelerated stress tests. These tests can assess the true lifetime of a catalyst under normal operating conditions, but in a significantly reduced length of time[275]. This is not straightforward, as simply increasing the current applied to the system does not necessarily yield a proportional reduction in the catalyst lifetime. In fact, the root cause of the electrochemical cell's instability can change when operating at the accelerated conditions.

***Circular hydrogen economy.*** Hydrogen produced via water electrolysis is key for the energy transition our society is going through, considering its role for energy storage, fuel and bulk chemical production. FIGURE 7 illustrates a hydrogen economy where hydrogen from water is produced using renewable electricity[11]. This hydrogen can be stored when energy demand is low and utilized when energy demand is high in the transportation, industrial and residential sectors[10,11]. To offset a significant amount of $CO_2$ emissions, renewable hydrogen can be used in the Haber–Bosch process to synthesize ammonia[276], which can then be used in the agriculture sector as fertilizer or as fuel in the transportation sector. When ammonia is used in fuel cells, it generates electricity and releases $N_2$ and valuable hydrogen as by-products[277–279]. The hydrogen can then be re-converted to ammonia or injected back into the hydrogen economy. Hydrogen can also be used to synthesize hydrocarbon liquid carriers; however, one caveat with hydrocarbon liquid carriers is that when used in the fuel cell, the oxidation of hydrocarbons releases $CO_2$. Achieving global electrification will require serious breakthroughs in the different industrial

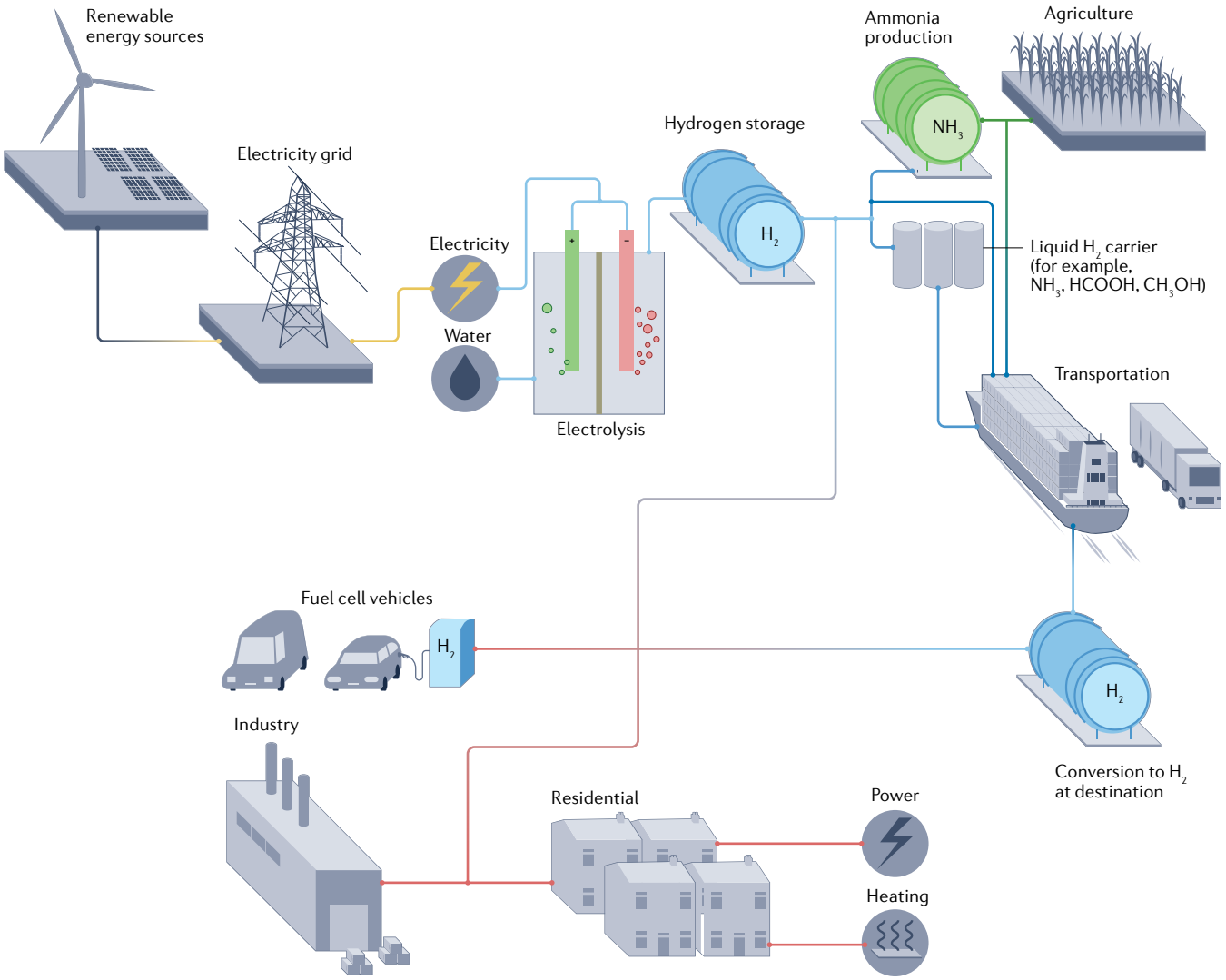


Fig. 7 | **Overview of the hydrogen economy.** Hydrogen produced from renewable water electrolysis can be utilized as a $CO_2$-neutral source in the agricultural, transportation, industrial and residential sectors.

sectors and, importantly, in society. For instance, storage of renewable energy as hydrogen is crucial to enable sustainable mobility of trucks and planes, whereas electric alternatives are currently impractical due to the low energetic density of batteries. Hence, the future of electrochemical water splitting is bright, and bridging fundamental and applied electrochemistry towards practical applications is urgent and necessary.

Published online: 27 October 2022


1. Pehl, M. et al. Understanding future emissions from low-carbon power systems by integration of life-cycle assessment and integrated energy modelling. *Nat. Energy* **2**, 939–945 (2017).
2. Berrang-Ford, L. et al. Tracking global climate change adaptation among governments. *Nat. Clim. Chang.* **9**, 440–449 (2019).
3. Bogdanov, D. et al. Low-cost renewable electricity as the key driver of the global energy transition towards sustainability. *Energy* **227**, 120467 (2021).
4. Lèbre, É. et al. The social and environmental complexities of extracting energy transition metals. *Nat. Commun.* **11**, 1–8 (2020).
5. Akcil, A., Sun, Z. & Panda, S. COVID-19 disruptions to tech-metals supply are a wake-up call. *Nature* **587**, 365–367 (2020).
6. Herrington, R. Mining our green future. *Nat. Rev. Mater.* **6**, 456–458 (2021).
7. Bamana, G., Miller, J. D., Young, S. L. & Dunn, J. B. Addressing the social life cycle inventory analysis data gap: Insights from a case study of cobalt mining in the Democratic Republic of the Congo. *One Earth* **4**, 1704–1714 (2021).
8. Majumdar, A., Deutch, J. M., Prasher, R. S. & Griffin, T. P. A framework for a hydrogen economy. *Joule* **5**, 1905–1908 (2021).
9. Pingkuo, L. & Xue, H. Comparative analysis on similarities and differences of hydrogen energy development in the world's top 4 largest economies: a novel framework. *Int. J. Hydrog. Energy* **47**, 9485–9503 (2022).
10. Crabtree, G. W., Dresselhaus, M. S. & Buchanan, M. V. The hydrogen economy. *Phys. Today* **57**, 39–45 (2004).
11. Bockris, J. O. A hydrogen economy. *Science* **176**, 1323 (1972).
12. Ihara, S. Feasibility of hydrogen production by direct water splitting at high temperature. *Int. J. Hydrog. Energy* **3**, 287–296 (1978).
13. Boettcher, S. W. et al. Potentially confusing: potentials in electrochemistry. *ACS Energy Lett.* **6**, 261–266 (2021).
14. Hansen, J. N. et al. Is there anything better than Pt for HER? *ACS Energy Lett.* **6**, 1175–1180 (2021).
15. Kothari, R., Buddhi, D. & Sawhney, R. L. Comparison of environmental and economic aspects of various hydrogen production methods. *Renew. Sustain. Energy Rev.* **12**, 553–563 (2008).
16. McCrory, C. C. L. et al. Benchmarking hydrogen evolving reaction and oxygen evolving reaction electrocatalysts for solar water splitting devices. *J. Am. Chem. Soc.* **137**, 4347–4357 (2015). **This work utilizes the protocol from Koper at al. to compare the activity, stability, electrochemically active surface area and Faradic efficiency of ten electrocatalysts for the OER.**
17. Bard, A. J. & Faulkner, L. R. *Electrochemical Methods: Fundamentals and Applications* (Wiley, 2001).
18. Elgrishi, N. et al. A practical beginner's guide to cyclic voltammetry. *J. Chem. Educ.* **95**, 197–206 (2018).
19. Norskov, J., Bligaard, T., Abild-Pedersen, F. & Studt, F. *Fundamental Concepts in Heterogeneous Catalysis* (Wiley, 2010).

20. Tanaka, Y. *Ion Exchange Membranes: Fundamentals and Applications* (Elsevier Science, 2015).
21. Luo, T., Abdu, S. & Wessling, M. Selectivity of ion exchange membranes: a review. *J. Memb. Sci.* **555**, 429–454 (2018).
22. Oener, S. Z., Foster, M. J. & Boettcher, S. W. Accelerating water dissociation in bipolar membranes and for electrocatalysis. *Science* **369**, 1099–1103 (2020).
23. Tiwari, A., Maagaard, T., Chorkendorff, I. & Horch, S. Effect of dissolved glassware on the structure-sensitive part of the Cu(111) voltammogram in KOH. *ACS Energy Lett.* **4**, 1645–1649 (2019).
24. Mayrhofer, K. J. J., Wiberg, G. K. H. & Arenz, M. Impact of glass corrosion on the electrocatalysis on Pt electrodes in alkaline electrolyte. *J. Electrochem. Soc.* **155**, P1–P5 (2008).
25. Mayrhofer, K. J. J., Crampton, A. S., Wiberg, G. K. H. & Arenz, M. Analysis of the impact of individual glass constituents on electrocatalysis on Pt electrodes in alkaline solution. *J. Electrochem. Soc.* **155**, P78–P81 (2008).
**This work demonstrates the impact of dissolved glassware on the reproducibility of studies using platinum single crystal surfaces in alkaline media**.
26. Fatiadi, A. J. The classical permanganate ion: still a novel oxidant in organic chemistry. *Synthesis* **1987**, 85–127 (1987).
27. Shaabani, A., Tavasoli-Rad, F. & Lee, D. G. Potassium permanganate oxidation of organic compounds. *Synth. Commun.* **35**, 571–580 (2005).
28. Arulmozhi, N., Esau, D., van Drunen, J. & Jerkiewicz, G. Design and development of instrumentations for the preparation of platinum single crystals for electrochemistry and electrocatalysis research part 3: final treatment, electrochemical measurements, and recommended laboratory practices. *Electrocatalysis* **9**, 113–123 (2018).
29. IKA. General guidelines for cleaning electrodes. *IKA* https://www.ika.com/ika/pdf/flyer-catalog/202103_Electrasyn%202.0_cleaning%20electrodes_EN.pdf (2021).
30. Kiema, G. K., Aktay, M. & Mcdermott, M. T. Preparation of reproducible glassy carbon electrodes by removal of polishing impurities. *J. Electroanal. Chem.* **540**, 7–15 (2003).
31. Monteiro, M. C. O. & Koper, M. T. M. Alumina contamination through polishing and its effect on hydrogen evolution on gold electrodes. *Electrochim. Acta* **325**, 134915 (2019).
**This work demonstrates how contamination introduced during polishing of electrodes affects the activity for the HER**.
32. Raaijman, S. J., Arulmozhi, N., Silva, A. H. M. & Koper, M. T. M. Clean and reproducible voltammetry of copper single crystals with prominent facet-specific features using induction annealing. *J. Electrochem. Soc.* **168**, 096510 (2021).
33. Kibler, L. A. *Preparation and characterization of noble metal single crystal electrode surfaces* (International Society of Electrochemistry, 2003).
**This paper presents a comprehensive guide on the preparation and characterization of noble metal single crystal surfaces for fundamental electrocatalysis studies**.
34. Seh, Z. W. et al. Combining theory and experiment in electrocatalysis: Insights into materials design. *Science* **355**, 6321 (2017).
35. Shinozaki, K., Zack, J. W., Pylypenko, S., Pivovar, B. S. & Kocha, S. S. Oxygen reduction reaction measurements on platinum electrocatalysts utilizing rotating disk electrode technique II. Influence of ink formulation, catalyst layer uniformity and thickness. *J. Electrochem. Soc.* **162**, F1384–F1396 (2015).
36. Morales, D. M., Villalobos, J., Kazakova, M. A., Xiao, J. & Risch, M. Nafion-Induced reduction of manganese and its impact on the electrocatalytic properties of a highly active MnFeNi oxide for bifunctional oxygen conversion. *ChemElectroChem* **8**, 2979–2983 (2021).
37. Jervis, R. et al. The importance of using alkaline ionomer binders for screening electrocatalysts in alkaline electrolyte. *J. Electrochem. Soc.* **164**, F1551–F1555 (2017).
**This paper presents guidelines for appropriate ionomer binder choice for screening catalysts in alkaline media**.
38. Birdja, Y. Y. et al. Effects of substrate and polymer encapsulation on $CO_2$ electroreduction by immobilized indium(III) protoporphyrin. *ACS Catal.* **8**, 4420–4428 (2018).
39. Garsany, Y., Ge, J., St-Pierre, J., Rocheleau, R. & Swider-Lyons, K. E. Analytical procedure for accurate comparison of rotating disk electrode results for the oxygen reduction activity of Pt/C. *J. Electrochem. Soc.* **161**, F628–F640 (2014).
40. Jerkiewicz, G. Applicability of platinum as a counter-electrode material in electrocatalysis research. *ACS Catal.* **12**, 2661–2670 (2022).
41. Chen, R. et al. Use of platinum as the counter electrode to study the activity of nonprecious metal catalysts for the hydrogen evolution reaction. *ACS Energy Lett.* **2**, 1070–1075 (2017).
42. Lee, J. & Bang, J. H. Reliable counter electrodes for the hydrogen evolution reaction in acidic media. *ACS Energy Lett.* **5**, 2706–2710 (2020).
43. Bird, M. A., Goodwin, S. E. & Walsh, D. A. Best practice for evaluating electrocatalysts for hydrogen economy. *ACS Appl. Mater. Interfaces* **12**, 20500–20506 (2020).
**This work recommends carbon counter electrodes separated from the working electrode compartment by a frit to avoid cross-contamination in studies of the HER**.
44. Ji, S. G., Kim, H., Park, C., Kim, W. & Choi, C. H. Underestimation of platinum electrocatalysis induced by carbon monoxide evolved from graphite counter electrodes. *ACS Catal.* **10**, 10773–10783 (2020).
45. Jerkiewicz, G. Standard and reversible hydrogen electrodes: theory, design, operation, and applications. *ACS Catal.* **10**, 8409–8417 (2020).
46. Nu, S., Li, S., Du, Y., Han, X. & Xu, P. How to reliably report the overpotential of an electrocatalyst. *ACS Energy Lett.* **5**, 1083–1087 (2020).
47. Leung, K. Y. & Mccrory, C. C. L. Effect and prevention of trace $Ag^+$ contamination from Ag/AgCl reference electrodes on $CO_2$ reduction product distributions at polycrystalline copper electrodes. *ACS Appl. Energy Mater.* **2**, 8283–8293 (2019).
48. Roger, I. & Symes, M. D. Silver leakage from Ag/AgCl reference electrodes as a potential cause of interference in the electrocatalytic hydrogen evolution reaction. *ACS Appl. Mater. Interfaces* **9**, 472–478 (2017).
49. Mousavi, M. P. S., Saba, S. A., Anderson, E. L., Hillmyer, M. A. & Bühlmann, P. Avoiding errors in electrochemical measurements: effect of frit material on the performance of reference electrodes with porous frit junctions. *Anal. Chem.* **88**, 8706–8713 (2016).
50. Zeledón, J. A. Z., Jackson, A., Stevens, M. B., Kamat, G. A. & Jaramillo, T. F. Methods — a practical approach to the reversible hydrogen electrode scale. *J. Electrochem. Soc.* **169**, 066505 (2022).
51. Rosca, V., Duca, M., de Groot, M. T. & Koper, M. T. M. Nitrogen cycle electrocatalysis. *Chem. Rev.* **109**, 2209–2244 (2009).
52. Subbaraman, R. et al. Origin of anomalous activities for electrocatalysts in alkaline electrolytes. *J. Phys. Chem. C.* **116**, 22231–22237 (2012).
53. Kodama, K., Jinnouchi, R., Takahashi, N., Murata, H. & Morimoto, Y. Activities and stabilities of Au-modified stepped-Pt single-crystal electrodes as model cathode catalysts in polymer electrolyte fuel cells. *J. Am. Chem. Soc.* **138**, 4194–4200 (2016).
54. Trotochaud, L., Young, S. L., Ranney, J. K. & Boettcher, S. W. Nickel–iron oxyhydroxide oxygen-evolution electrocatalysts: the role of intentional and incidental iron incorporation. *J. Am. Chem. Soc.* **136**, 6744–6753 (2014).
55. Corrigan, D. A. The catalysis of the oxygen evolution reaction by iron impurities in thin film nickel oxide electrodes. *J. Electrochem. Soc.* **134**, 377–384 (1987).
56. Ojha, K., Doblhoff-Dier, K. & Koper, M. T. M. Double-layer structure of the Pt(111)–aqueous electrolyte interface. *Proc. Natl Acad. Sci. USA* **119**, e2116016119 (2022).
57. Sheberla, D. et al. Conductive MOF electrodes for stable supercapacitors with high areal capacitance. *Nat. Mater.* **16**, 220–225 (2017).
58. Wuttig, A. & Surendranath, Y. Impurity ion complexation enhances carbon dioxide reduction catalysis. *ACS Catal.* **5**, 4479–4484 (2015).
59. Spanos, I. et al. Facile protocol for alkaline electrolyte purification and its influence on a Ni–Co oxide catalyst for the oxygen evolution reaction. *ACS Catal.* **9**, 8165–8170 (2019).
60. Liu, L. et al. Purification of residual Ni and Co hydroxides from Fe-free alkaline electrolyte for electrocatalysis studies. *ChemElectroChem* https://doi.org/10.1002/celc.202200279 (2022).
61. Rebollar, L., Intikhab, S., Snyder, J. D. & Tang, M. H. Kinetic isotope effects quantify pH-sensitive water dynamics at the Pt electrode interface. *J. Phys. Chem. L* **11**, 2308–2313 (2020).
62. Anderson, C. E. & Ebenhaek, D. G. in *Analysis of Essential Nuclear Reactor Materials* (ed. Rodden, C. J.) 629–661 (US Atomic Energy Commission, 1964).
63. Schmidt, T. J. et al. Characterization of high-surface-area electrocatalysts using a rotating disk electrode configuration. *J. Electrochem. Soc.* **145**, 2354–2358 (1998).
64. Levich, V. G. in *Physicochemical Hydrodynamics* 60–72 (Prentice-Hall Englewood, 1962).
65. Villullas, H. M. & Lopez Teijelo, M. Meniscus shape and lateral wetting at the hanging meniscus rotating disc (HMRD) electrode. *J. Appl. Electrochem.* **26**, 353–359 (1996).
66. Janssen, L. J. J., Sillen, C. W. M. P., Barendrecht, E. & van Stralen, S. J. D. Bubble behaviour during oxygen and hydrogen evolution at transparent electodes in KOH solution. *Electrochim. Acta* **29**, 633–642 (1984).
67. Matsuura, K., Yamanishi, Y., Guan, C. & Yanase, S. Control of hydrogen bubble plume during electrolysis of water. *J. Phys. Commun.* **3**, 035012 (2019).
68. Hodges, A. et al. A high-performance capillary-fed electrolysis cell promises more cost-competitive renewable hydrogen. *Nat. Commun.* **13**, 1304 (2022).
69. Zhao, X., Ren, H. & Luo, L. Gas bubbles in electrochemical gas evolution reactions. *Langmuir* **35**, 5392–5408 (2019).
70. Angulo, A., Linde, P., van der, Gardeniers, H., Modestino, M. & Rivas, D. F. Influence of bubbles on the energy conversion efficiency of electrochemical reactors. *Joule* **4**, 555–579 (2020).
**This work demonstrates how bubbles impact the energy efficiency of electrocatalytic processes**.
71. Zdunek, A. D. & Selman, J. R. A novel rotating disk electrode cell design: the inverted rotating disk. *J. Electrochem. Soc.* **139**, 2549–2551 (1992).
72. Meethal, R. P., Saibi, R. & Srinivasan, R. Hydrogen evolution reaction on polycrystalline Au inverted rotating disc electrode in $HClO_4$ and NaOH solutions. *Int. J. Hydrog. Energy* **47**, 14304–14318 (2022).
73. Vos, J. G. & Koper, M. T. M. Examination and prevention of ring collection failure during gas-evolving reactions on a rotating ring-disk electrode. *J. Electroanal. Chem.* **850**, 113363 (2019).
74. Shih, A. J., Arulmozhi, N. & Koper, M. T. M. Electrocatalysis under cover: enhanced hydrogen evolution via defective graphene-covered Pt(111). *ACS Catal.* **11**, 10892–10901 (2021).
75. Hsu, J. P. Recommended pre-operation cleanup procedures for hydrogen fueling station. *Int. J. Hydrog. Energy* **37**, 1770–1780 (2011).
76. Wan, C. T. et al. A potential-dependent Thiele modulus to quantify the effectiveness of porous electrocatalysts. Preprint at https://doi.org/10.26434/chemrxiv-2021-cwqm0-v2 (2021).
**This work demonstrates the coupling of diffusion reaction-governing equations with macroscopic catalytic rates to quantify the extent of internal mass transfer limitations**.
77. Hickman, D. A., Degenstein, J. C. & Ribeiro, F. H. Fundamental principles of laboratory fixed bed reactor design. *Curr. Opin. Chem. Eng.* **13**, 1–9 (2016).
78. Harris, J. W. et al. Consequences of product inhibition in the quantification of kinetic parameters. *J. Catal.* **389**, 468–475 (2020).
79. Kamat, G. A. et al. Acid anion electrolyte effects on platinum for oxygen and hydrogen electrocatalysis. *Commun. Chem.* **5**, 1–10 (2022).
80. Zhang, Y., Zhang, H., Ji, H., Chen, C. & Zhao, J. Pivotal role and regulation of proton transfer in water oxidation on hematite photoanodes. *J. Am. Chem. Soc.* **138**, 2705–2711 (2016).
81. Yang, H. et al. Intramolecular hydroxyl nucleophilic attack pathway by a polymeric water oxidation catalyst with single cobalt sites. *Nat. Catal.* **5**, 414–429 (2022).
82. Chen, Z. et al. Concerted O atom-proton transfer in the O–O bond forming step in water oxidation. *Proc. Natl Acad. Sci. USA* **107**, 7225–7229 (2010).
83. Xia, C. et al. Confined local oxygen gas promotes electrochemical water oxidation to hydrogen peroxide. *Nat. Catal.* **3**, 125–134 (2020).
84. Rabe, M. et al. Alkaline manganese electrochemistry studied by in situ and operando spectroscopic methods — metal dissolution, oxide formation and oxygen evolution. *Phys. Chem. Chem. Phys.* **21**, 10457–10469 (2019).
85. Huang, J. et al. In situ monitoring of the electrochemically induced phase transition of thermodynamically metastable 1T-$MoS_2$ at nanoscale. *Nanoscale* **12**, 9246–9254 (2020).

86. Shpigel, N., Levi, M. D., Sigalov, S., Daikhin, L. & Aurbach, D. In situ real-time mechanical and morphological characterization of electrodes for electrochemical energy storage and conversion by electrochemical quartz crystal microbalance with dissipation monitoring. *Acc. Chem. Res.* **51**, 69–79 (2018).
87. Hodnik, N., Dehm, G. & Mayrhofer, K. J. J. Importance and challenges of electrochemical in situ liquid cell electron microscopy for energy conversion research. *Acc. Chem. Res.* **49**, 2015–2022 (2016).
**This work applies in situ liquid cell electron microscopy for electrocatalysis research**.
88. Velasco-Velez, J.-J. et al. Revealing the active phase of copper during the electroreduction of $CO_2$ in aqueous electrolyte by correlating in situ X-ray spectroscopy and in situ electron microscopy. *ACS Energy Lett.* **5**, 2106–2111 (2020).
89. Zhang, L., Shi, W. & Zhang, B. A review of electrocatalyst characterization by transmission electron microscopy. *J. Energy Chem.* **26**, 1117–1135 (2017).
90. Timoshenko, J. & Roldan Cuenya, B. In situ/operando electrocatalyst characterization by X-ray absorption spectroscopy. *Chem. Rev.* **121**, 882–961 (2021).
**This work applies in situ and operando XAS to probe the interactions of working electrocatalysts with the environment and its structural, chemical and electronic transformations**.
91. Velasco-Velez, J.-J. et al. A comparative study of electrochemical cells for in situ X-ray spectroscopies in the soft and tender X-ray range. *J. Phys. D. Appl. Phys.* **54**, 124003 (2021).
92. Liu, Y. et al. Transition metal nitrides as promising catalyst supports for tuning $CO/H_2$ syngas production from electrochemical $CO_2$ reduction. *Angew. Chem. Int. Ed.* **59**, 11345–11348 (2020).
93. Sasaki, K., Marinkovic, N., Isaacs, H. S. & Adzic, R. R. Synchrotron-based in situ characterization of carbon-supported platinum and platinum monolayer electrocatalysts. *ACS Catal.* **6**, 69–76 (2016).
94. Sugawara, Y., Yadav, A. P., Nishikata, A. & Tsuru, T. Electrochemical quartz crystal microbalance study on dissolution of platinum in acid solutions. *Electrochemistry* **75**, 359–365 (2007).
95. Levi, M. D., Salitra, G., Levy, N., Aurbach, D. & Maier, J. Application of a quartz-crystal microbalance to measure ionic fluxes in microporous carbons for energy storage. *Nat. Mater.* **8**, 872–875 (2009).
96. Wang, Y.-H. et al. In situ Raman spectroscopy reveals the structure and dissociation of interfacial water. *Nature* **600**, 81–85 (2021).
**This research paper provides modelling guidelines to assess the structure of the electrochemical interface including water, cations and electric field. Theoretical results are benchmarked through in situ Raman spectroscopy characterization**.
97. Dong, J.-C. et al. In situ Raman spectroscopic evidence for oxygen reduction reaction intermediates at platinum single-crystal surfaces. *Nat. Energy* **4**, 60–67 (2019).
98. Liang, Y. et al. Electrochemical scanning probe microscopies in electrocatalysis. *Small Methods* **3**, 1800387 (2019).
99. Simon, G. H., Kley, C. S. & Roldan Cuenya, B. Potential-dependent morphology of copper catalysts during $CO_2$ electroreduction revealed by in situ atomic force microscopy. *Angew. Chem. Int. Ed.* **60**, 2561–2568 (2021).
100. Li, J. F., Zhang, Y. J., Ding, S. Y., Panneerselvam, R. & Tian, Z. Q. Core-shell nanoparticle-enhanced raman spectroscopy. *Chem. Rev.* **117**, 5002–5069 (2017).
101. Kas, R., Ayemoba, O., Firet, N. J., Middelkoop, J. & Smith, W. A. In-situ infrared spectroscopy applied to the study of the electrocatalytic reduction of $CO_2$: theory, practice and challenges. *ChemPhysChem* **20**, 2904–2925 (2019).
102. Zhu, S., Li, T., Cai, W.-B. & Shao, M. $CO_2$ electrochemical reduction as probed through infrared spectroscopy. *ACS Energy Lett.* **4**, 682–689 (2019).
103. Zhang, Z.-Q., Banerjee, S., Thoi, V. S. & Shoji Hall, A. Reorganization of interfacial water by an amphiphilic cationic surfactant promotes $CO_2$ reduction. *J. Phys. Chem. Lett.* **11**, 5457–5463 (2020).
104. Friebel, D. et al. Balance of nanostructure and bimetallic interactions in Pt model fuel cell catalysts: in situ XAS and DFT study. *J. Am. Chem. Soc.* **134**, 9664–9671 (2012).
105. Wu, C. H. et al. The structure of interfacial water on gold electrodes studied by X-ray absorption spectroscopy. *Science* **346**, 831–834 (2014).
106. Mom, R. et al. The oxidation of platinum under wet conditions observed by electrochemical X-ray photoelectron spectroscopy. *J. Am. Chem. Soc.* **141**, 6537–6544 (2019).
107. Velasco-Velez, J. J. et al. Photoelectron spectroscopy at the graphene–liquid interface reveals the electronic structure of an electrodeposited cobalt/graphene electrocatalyst. *Angew. Chem. Int. Ed.* **54**, 14554–14558 (2015).
108. Favaro, M. et al. An operando investigation of (Ni–Fe–Co–Ce)Ox system as highly efficient electrocatalyst for oxygen evolution reaction. *ACS Catal.* **7**, 1248–1258 (2017).
109. Ledezma-Yanez, I. et al. Interfacial water reorganization as a pH-dependent descriptor of the hydrogen evolution rate on platinum electrodes. *Nat. Energy* **2**, 17031 (2017).
110. Favaro, M. et al. Unravelling the electrochemical double layer by direct probing of the solid/liquid interface. *Nat. Commun.* **7**, 1–8 (2016).
111. Rao, R. R. et al. Operando identification of site-dependent water oxidation activity on ruthenium dioxide single-crystal surfaces. *Nat. Catal.* **3**, 516–525 (2020).
112. Reikowski, F. et al. Operando surface X-ray diffraction studies of structurally defined $Co_3O_4$ and CoOOH thin films during oxygen evolution. *ACS Catal.* **9**, 3811–3821 (2019).
113. Gründer, Y. & Lucas, C. A. Surface X-ray diffraction studies of single crystal electrocatalysts. *Nano Energy* **29**, 378–393 (2016).
114. Bogar, M. et al. Interplay among dealloying, ostwald ripening, and coalescence in PtXNi100–X bimetallic alloys under fuel-cell-related conditions. *ACS Catal.* **11**, 11360–11370 (2021).
115. Jacobse, L., Rost, M. J. & Koper, M. T. M. Atomic-scale identification of the electrochemical roughening of platinum. *ACS Cent. Sci.* **5**, 1920–1928 (2019).
116. Wang, X. et al. In situ scanning tunneling microscopy of cobalt-phthalocyanine-catalyzed $CO_2$ reduction reaction. *Angew. Chem.* **59**, 16098–16103 (2020).
117. Wang, X. et al. Mechanistic reaction pathways of enhanced ethylene yields during electroreduction of $CO_2$–CO co-feeds on Cu and Cu-tandem electrocatalysts. *Nat. Nanotechnol.* **14**, 1063–1070 (2019).
118. Davies, B. J. V., Arenz, M., Rossmeisl, J. & Escudero-Escribano, M. Electrochemical synthesis of high-value chemicals: detection of key reaction intermediates and products combining gas chromatography–mass spectrometry and in situ infrared spectroscopy. *J. Phys. Chem. C.* **123**, 12762–12772 (2019).
119. Kwon, Y. & Koper, M. T. M. Combining voltammetry with HPLC: application to electro-oxidation of glycerol. *Anal. Chem.* **82**, 5420–5424 (2010).
120. Zeng, R. et al. Methanol oxidation using ternary ordered intermetallic electrocatalysts: a DEMS study. *ACS Catal.* **10**, 770–776 (2020).
121. Stoerzinger, K. A. et al. Orientation-dependent oxygen evolution on $RuO_2$ without lattice exchange. *ACS Energy Lett.* **2**, 876–881 (2017).
122. Todoroki, N., Tsurumaki, H., Tei, H., Mochizuki, T. & Wadayama, T. Online electrochemical mass spectrometry combined with the rotating disk electrode method for direct observations of potential-dependent molecular behaviors in the electrode surface vicinity. *J. Electrochem. Soc.* **167**, 106503 (2020).
123. Geiger, S. et al. The stability number as a metric for electrocatalyst stability benchmarking. *Nat. Catal.* **1**, 508–515 (2018).
124. Lopes, P. P. et al. Relationships between atomic level surface structure and stability/activity of platinum surface atoms in aqueous environments. *ACS Catal.* **6**, 2536–2544 (2016).
125. Kasian, O. et al. Degradation of iridium oxides via oxygen evolution from the lattice: correlating atomic scale structure with reaction mechanisms. *Energy Environ. Sci.* **12**, 3548–3555 (2019).
126. Klemm, S. O., Topalov, A. A., Laska, C. A. & Mayrhofer, K. J. J. Coupling of a high throughput microelectrochemical cell with online multielemental trace analysis by ICP-MS. *Electrochem. Commun.* **13**, 1533–1535 (2011).
127. Kunimatsu, K., Senzaki, T., Samejeske, G., Tsushima, M. & Osawa, M. Hydrogen adsorption and hydrogen evolution reaction on a polycrystalline Pt electrode studied by surface-enhanced infrared absorption spectroscopy. *Electrochim. Acta* **52**, 5715–5724 (2007).
128. Scott, S. B. et al. The low overpotential regime of acidic water oxidation part I: the importance of $O_2$ detection. *Energy Environ. Sci.* https://doi.org/10.1039/d1ee03914h (2022).
129. Yokoyama, Y. et al. In situ local pH measurements with hydrated iridium oxide ring electrodes in neutral pH aqueous solutions. *Chem. Lett.* **49**, 195–198 (2020).
130. Monteiro, M. C. O., Liu, X., Hagedoorn, B. J. L., Snabilié, D. D. & Koper, M. T. M. Interfacial pH measurements using a rotating ring-disc electrode with a voltammetric pH sensor. *ChemElectroChem* **9**, e202101223 (2022).
131. Grimaud, A. et al. Activating lattice oxygen redox reactions in metal oxides to catalyse oxygen evolution. *Nat. Chem.* **9**, 457–465 (2017).
132. Čolić, V. et al. Experimental aspects in benchmarking of the electrocatalytic activity. *ChemElectroChem* **2**, 143–149 (2015).
133. Zheng, J., Yan, Y. & Xu, B. Correcting the hydrogen diffusion limitation in rotating disk electrode measurements of hydrogen evolution reaction kinetics. *J. Electrochem. Soc.* **162**, F1470–F1481 (2015).
134. Wei, C. et al. Recommended practices and benchmark activity for hydrogen and oxygen electrocatalysis in water splitting and fuel cells. *Adv. Mater.* **31**, 1806296 (2019).
**This work expands our coverage on the collection and analysis of reaction rates, kinetics and normalization of catalyst activity**.
135. Voiry, D. et al. Best practices for reporting electrocatalytic performance of nanomaterials. *ACS Nano* **12**, 9635–9638 (2018).
136. Prats, H. & Chan, K. The determination of the HOR/HER reaction mechanism from experimental kinetic data. *Phys. Chem. Chem. Phys.* https://doi.org/10.1039/d1cp04134g (2021).
137. Wei, C., Sun, S., Mandler, D. & Wang, X. Approaches for measuring the surface areas of metal oxide electrocatalysts for determining their intrinsic electrocatalytic activity. *Chem Soc Rev.* https://doi.org/10.1039/c8cs00848e (2019).
138. Garreau, D. & Saveant, J. M. Linear sweep voltammetry — compensation of cell resistance and stability. *Electroanal. Chem. Interfacial Electrochem.* **35**, 309–331 (1972).
139. Koutecky, J. & Levich, V. G. The application of the rotating disc electrode to studies of kinetic and catalytic processes. *Zh. Fiz. Khim.* **32**, 1565–1575 (1958).
140. Fogler, H. S. *Essentials of Chemical Reaction Engineering* (Pearson Education, 2010).
141. Monteiro, M. C. O., Jacobse, L., Touzalin, T. & Koper, M. T. M. Mediator-free SECM for probing the diffusion layer pH with functionalized gold ultramicroelectrodes. *Anal. Chem.* **92**, 2237–2243 (2020).
142. Monteiro, M. C. O. & Koper, M. T. M. Measuring local pH in electrochemistry. *Curr. Opin. Electrochem.* **25**, 100649 (2021).
143. Goyal, A. & Koper, M. T. M. Understanding the role of mass transport in tuning the hydrogen evolution kinetics on gold in alkaline media. *J. Chem. Phys.* **155**, 134705 (2021).
144. Hasan, M. H. & McCrum, I. T. Understanding the role of near-surface solvent in electrochemical adsorption and electrocatalysis with theory and experiment. *Curr. Opin. Electrochem.* **33**, 100937 (2022).
145. Taylor, H. S. The mechanism of activation at catalytic surfaces. *Proc. R. Soc. A Math. Phys. Eng. Sci.* **113**, 77–86 (1926).
146. Boudart, M. Turnover rates in heterogeneous catalysis. *Chem. Rev.* **95**, 661–666 (1995).
147. Kozuch, S. & Martin, J. M. L. "Turning Over" definitions in catalytic cycles. *ACS Catal.* **2**, 2787–2794 (2012).
148. Anantharaj, S., Karthik, P. E. & Noda, S. The significance of properly reporting turnover frequency in electrocatalysis research. *Angew. Chem. Int. Ed.* **60**, 23051–23067 (2021).
149. Barber, J., Morin, S. & Conway, B. E. Specificity of the kinetics of $H_2$ evolution to the structure of single-crystal Pt surfaces, and the relation between OPD and UPD H. *J. Electroanal. Chem.* **446**, 125–138 (1998).
150. Weber, R. S. Lies, damned lies, and turnover rates. *J. Catal.* **404**, 925–928 (2021).
151. Trasatti, S. & Petrii, O. A. Real surface area measurements in electrochemistry. *J. Electroanal. Chem.* **327**, 353–376 (1993).
152. Li, D., Batchelor-McAuley, C. & Compton, R. G. Some thoughts about reporting the electrocatalytic performance of nanomaterials. *Appl. Mater. Today* **18**, 100404 (2020).
153. Hou, S. et al. A review on experimental identification of active sites in model bifunctional electrocatalytic

systems for oxygen reduction and evolution reactions. *ChemElectroChem* **8**, 3433–3456 (2021).
154. Jaramillo, T. F. et al. Identification of active edge sites for electrochemical $H_2$ evolution from $MoS_2$ nanocatalysts. *Science* **317**, 100–103 (2007).
155. Anantharaj, S. & Kundu, S. Do the evaluation parameters reflect intrinsic activity of electrocatalysts in electrochemical water splitting? *ACS Energy Lett.* **4**, 1260–1264 (2019).
156. Stoerzinger, K. A., Qiao, L., Biegalski, M. D. & Shao-Horn, Y. Orientation-dependent oxygen evolution activities of rutile $IrO_2$ and $RuO_2$. *J. Phys. Chem. Lett.* **5**, 1636–1641 (2014).
157. Kluge, R. M., Haid, R. W. & Bandarenka, A. S. Assessment of active areas for the oxygen evolution reaction on an amorphous iridium oxide surface. *J. Catal.* **396**, 14–22 (2021).
158. Aufa, M. H. et al. Fast and accurate determination of the electroactive surface area of $MnO_x$. *Electrochim. Acta* **389**, 138692 (2021).
159. Watzele, S. & Bandarenka, A. S. Quick determination of electroactive surface area of some oxide electrode materials. *Electroanalysis* **28**, 2394–2399 (2016).
160. Watzele, S. et al. Determination of electroactive surface area of Ni-, Co-, Fe-, and Ir-based oxide electrocatalysts. *ACS Catal.* **9**, 9222–9230 (2019).
161. Quast, T. et al. Single particle nanoelectrochemistry reveals the catalytic oxygen evolution reaction activity of $Co_3O_4$ nanocubes. *Angew. Chem. Int. Ed.* **60**, 23444–23450 (2021).
162. Shinagawa, T., Garcia-Esparza, A. T. & Takanabe, K. Insight on Tafel slopes from a microkinetic analysis of aqueous electrocatalysis for energy conversion. *Sci. Rep.* **5**, 13801 (2015).
**This work utilizes microkinetic modelling to demonstrate how different rate-limiting steps and surface coverages impact Tafel slopes and reaction orders**.
163. Jung, O., Jackson, M. N., Bisbey, R. P., Kogan, N. E. & Surendranath, Y. Innocent buffers reveal the intrinsic pH- and coverage-dependent kinetics of the hydrogen evolution reaction on noble metals. *Joule* **6**, 476–493 (2022).
164. Mitchell, J. B., Shen, M., Twight, L. & Boettcher, S. W. Hydrogen-evolution-reaction kinetics pH dependence: is it covered? *Chem. Catal* https://doi.org/10.1016/j.checat.2022.02.001 (2022).
165. Vos, J. G., Venugopal, A., Smith, W. A. & Koper, M. T. M. Competition and selectivity during parallel evolution of bromine, chlorine and oxygen on $IrO_x$ electrodes. *J. Catal.* **389**, 99–110 (2020).
166. Satterfield, C. N. *Mass Transfer in Heterogeneous Catalysis* (MIT Press, 1970).
167. Monteiro, M. C. O., Goyal, A., Moerland, P. & Koper, M. T. M. Understanding cation trends for hydrogen evolution on platinum and gold electrodes in alkaline media. *ACS Catal.* **11**, 14328–14335 (2021).
168. Chen, Q., Solla-gullõn, J., Sun, S. & Feliu, J. M. The potential of zero total charge of Pt nanoparticles and polycrystalline electrodes with different surface structure: the role of anion adsorption in fundamental electrocatalysis. *Electrochim. Acta* **55**, 7982–7994 (2010).
169. Grgur, B. N., Marković, N. M. & Ross, P. N. Temperature-dependent oxygen electrochemistry on platinum low-index single crystal surfaces in acid solutions. *Can. J. Chem.* **75**, 1465–1471 (1997).
170. Gojković, S. L., Zečević, S. K. & Dražić, D. M. Oxygen reduction on iron. Part VII. Temperature dependence of oxygen reduction on passivated iron in alkaline solutions. *J. Electroanal. Chem.* **399**, 127–133 (1995).
171. Tang, Z. Q., Liao, L. W., Zheng, Y. L., Kang, J. & Chen, Y. X. Temperature effect on hydrogen evolution reaction at Au electrode. *Chin. J. Chem. Phys.* **25**, 469–474 (2012).
172. Kang, J., Lin, C. H., Yao, Y. & Chen, Y. X. Kinetic implication from temperature effect on hydrogen evolution reaction at Ag electrode. *Chin. J. Chem. Phys.* **27**, 63–68 (2014).
173. Watzele, S. A., Katzenmeier, L., Sabawa, J. P., Garlyyev, B. & Bandarenka, A. S. Electrochimica acta temperature dependences of the double layer capacitance of some solid/liquid and solid/solid electrified interfaces. An experimental study. *Electrochim. Acta* **391**, 138969 (2021).
174. Garcia-Araez, N., Climent, V. & Feliu, J. M. Temperature effects on platinum single-crystal electrodes. *Russ. J. Electrochem.* **48**, 271–280 (2012).
175. Marković, N. M. et al. Effect of temperature on surface processes at the Pt(111)–liquid interface: hydrogen adsorption, oxide formation, and CO oxidation. *J. Phys. Chem. B* **103**, 8568–8577 (1999).
176. Gomez, R., Orts, J. M., Alvarez-Ruiz, B. & Feliu, J. M. Effect of temperature on hydrogen adsorption on Pt(111), Pt(110), and Pt(100) electrodes. *J. Phys. Chem.* **108**, 228–238 (2004).
177. He, Z. D., Chen, Y. X., Santos, E. & Schmickler, W. The pre-exponential factor in electrochemistry. *Angew. Chem.- Int. Ed.* **57**, 7948–7956 (2018).
178. Vos, R. E. & Koper, M. T. M. The effect of temperature on the cation-promoted electrochemical $CO_2$ reduction on gold. *ChemElectroChem* **9**, e202200239 (2022).
179. Conway, B. E. & Wilkinson, D. P. Non-isothermal cell potentialas and evaluation of entropies of ions and of activation for single electrode processes in non-aqueous media. *Electrochim. Acta* **38**, 997–1013 (1993).
180. Conway, B. E. & Wilkinsont, D. P. Comparison of entropic and enthalpic components of the barrier symmetry factor, $\beta$, for proton discharge at liquid and solid Hg in relation to the variation of Tafel slopes and $\beta$ with temperature. *J. Chem. Soc. Faraday Trans.* **85**, 2355–2367 (1989).
181. Wildgoose, G. G., Giovanelli, D., Lawrence, N. S. & Compton, R. G. High-temperature electrochemistry: a review. *Electroanalysis* **16**, 421–433 (2004).
182. Uwitonze, N., Chen, W., Zhou, D., He, Z. & Chen, Y.-X. The determination of thermal junction potential difference. *Sci. China Chem.* **61**, 1020–1024 (2018).
183. Öijerholm, J., Forsberg, S., Hermansson, H.-P. & Ullberg, M. Relation between the SHE and the internal Ag/AgCl reference electrode at high temperatures. *J. Electrochem. Soc.* **156**, P56–P61 (2009).
184. National Institute of Standards and Technology. IUPAC-NIST solubility database, version 1.1. NIST standard reference database 106. *SRDTA* https://doi.org/10.18434/T4QC79 (2012).
185. Williams, K., Limaye, A., Weiss, T., Chung, M. & Manthiram, K. Accounting for species' thermodynamic activities changes mechanistic interpretations of electrochemical kinetic data. Preprint at https://doi.org/10.26434/chemrxiv-2022-vk5z9 (2022).
**This work demonstrates how accounting for the thermodynamic activities of species can impact reaction order measurements, potentially leading to faulty mechanistic interpretations**.
186. Haschke, S. et al. Direct oxygen isotope effect identifies the rate-determining step of electrocatalytic OER at an oxidic surface. *Nat. Commun.* https://doi.org/10.1038/s41467-018-07031-1 (2018).
187. Pasquini, C. et al. H/D isotope effects reveal factors controlling catalytic activity in Co-based oxides for water oxidation. *J. Am. Chem. Soc.* **141**, 2938–2948 (2019).
188. Tse, E. C. M., Hoang, T. T. H., Varnell, J. A. & Gewirth, A. A. Observation of an inverse kinetic isotope effect in oxygen evolution electrochemistry. *ACS Catal.* **6**, 5706–5714 (2016).
189. Nørskov, J. K. et al. Trends in the exchange current for hydrogen evolution. *J. Electrochem. Soc.* **152**, J23–J26 (2005).
190. McCrum, I. T. & Koper, M. T. M. The role of adsorbed hydroxide in hydrogen evolution reaction kinetics on modified platinum. *Nat. Energy* **5**, 891–899 (2020).
**This research paper introduces *OH adsorption strength as an additional descriptor for HER activity in addition to *H binding, and also provides guidelines for assessing the kinetics of the HER in alkaline media and in the presence of cations**.
191. Koper, M. T. M. Thermodynamic theory of multi-electron transfer reactions: implications for electrocatalysis. *J. Electroanal. Chem.* **660**, 254–260 (2011).
192. Katayama, Y. et al. An in situ surface-enhanced infrared absorption spectroscopy study of electrochemical $CO_2$ reduction: selectivity dependence on surface C-bound and O-bound reaction intermediates. *J. Phys. Chem. C.* **123**, 5951–5963 (2019).
193. Feibelman, P. J. Surface-diffusion mechanism versus electric field: Pt/Pt(001). *Phys. Rev. B Condens. Matter Mater. Phys.* **64**, 125403 (2001).
194. Nørskov, J. K. et al. Origin of the overpotential for oxygen reduction at a fuel-cell cathode. *J. Phys. Chem. B* **108**, 17886–17892 (2004).
195. Tang, W., Sanville, E. & Henkelman, G. A grid-based Bader analysis algorithm without lattice bias. *J. Phys. Condens. Matter* **21**, 1–7 (2009).
196. Henkelman, G. A fast and robust algorithm for Bader decomposition of charge density. *Comput. Mater. Sci.* **36**, 354–360 (2006).
197. Sanville, E., Kenny, S. D., Smith, R. & Henkelman, G. Improved grid-based algorithm for bader charge allocation. *J. Comput. Chem.* **28**, 899–908 (2007).
198. Chen, L. D., Urushihara, M., Chan, K. & Nørskov, J. K. Electric field effects in electrochemical $CO_2$ reduction. *ACS Catal.* **6**, 7133–7139 (2016).
199. Monteiro, M. C. O., Dattila, F., Lopez, N. & Koper, M. T. M. The role of cation acidity on the competition between hydrogen evolution and $CO_2$ reduction on gold electrodes. *J. Am. Chem. Soc.* **144**, 1589–1602 (2022).
200. Gupta, N., Gattrell, M. & Macdougall, B. Calculation for the cathode surface concentrations in the electrochemical reduction of $CO_2$ in $KHCO_3$ solutions. *J. Appl. Elecrochem.* **36**, 161–172 (2006).
201. Weng, L.-C., Bell, A. T. & Weber, A. Z. Modeling gas-diffusion electrodes for $CO_2$ reduction. *Phys. Chem. Chem. Phys.* **20**, 16973–16984 (2018).
202. Cheng, D. et al. The nature of active sites for carbon dioxide electroreduction over oxide-supported copper catalysts. *Nat. Commun.* **12**, 395 (2021).
203. Pérez-Ramírez, J. & López, N. Strategies to break linear scaling relationships. *Nat. Catal.* **2**, 971–976 (2019).
204. Rossmeisl, J., Logadottir, A. & Nørskov, J. K. Electrolysis of water on (oxidized) metal surfaces. *Chem. Phys.* **319**, 178–184 (2005).
205. Rossmeisl, J., Qu, Z.-W., Zhu, H., Kroes, G.-J. & Norskov, J. K. Electrolysis of water on oxide surfaces. *J. Electroanal. Chem.* **607**, 83–89 (2007).
206. Brönsted, J. N. Acid and basic catalysis. *Chem. Rev.* **5**, 231–338 (1928).
207. Evans, M. G. & Polanyi, M. Inertia and driving force of chemical reaction. *Trans. Faraday Soc.* **34**, 11–24 (1938).
208. Bligaard, T. et al. The Brønsted–Evans–Polanyi relation and the volcano curve in heterogeneous catalysis. *J. Catal.* **224**, 206–217 (2004).
209. Man, I. C. et al. Universality in oxygen evolution electrocatalysis on oxide surfaces. *ChemCatChem* **3**, 1159–1165 (2011).
210. Goyal, A. & Koper, M. T. M. The interrelated effect of cations and electrolyte pH on the hydrogen evolution reaction on gold electrodes in alkaline media. *Angew. Chem. Int. Ed.* **60**, 13452–13462 (2021).
211. Ong, S. P. et al. Python Materials Genomics (pymatgen): a robust, open-source Python library for materials analysis. *Comput. Mater. Sci.* **68**, 314–319 (2013).
212. Gunasooriya, G. T. K. K., Nørskov, J. K. Analysis of acid-stable and active oxides for the oxygen evolution reaction. *ACS Energy Lett.* **5**, 3778–3787 (2020).
213. Zhou, L. et al. Rutile alloys in the Mn–Sb–O system stabilize $Mn^{3+}$ to enable oxygen evolution in strong acid. *ACS Catal.* **8**, 10938–10948 (2018).
214. Gunasooriya, G. T. K. K. et al. First-row transition metal antimonates for the oxygen reduction reaction. *ACS Nano* **16**, 6334–6348 (2022).
215. Kastlunger, G., Lindgren, P. & Peterson, A. A. Controlled-potential simulation of elementary electrochemical reactions: proton discharge on metal surfaces. *J. Phys. Chem. C.* **122**, 12771–12781 (2018).
216. Warburton, R. E., Soudackov, A. V. & Hammes-Schiffr, S. Theoretical modeling of electrochemical proton-coupled electron transfer. *Chem. Rev.* https://doi.org/10.1021/acs.chemrev.1c00929 (2022).
217. Abidi, N., Lim, K. R. G., Seh, Z. W. & Steinmann, S. N. Atomistic modeling of electrocatalysis: are we there yet? *WIREs Comput. Mol. Sci.* **11**, e1499 (2021).
**This outstanding review paper offers a detailed discussion on the different methodologies developed to model the electrochemical interface, including the computational hydrogen electrode, constant potential and constant electric field approaches (as summarized in the paper in Fig. 3)**.
218. Sundararaman, R., Vigil-fowler, D. & Schwarz, K. Improving the accuracy of atomistic simulations of the electrochemical interface. *Chem. Rev.* **122**, 10651–10674 (2022).
219. Groß, A. & Sakong, S. Ab initio simulations of water/metal interfaces. *Chem. Rev.* **122**, 10746–10776 (2022).
220. Pohlmann, S. Metrics and methods for moving from research to innovation in energy storage. *Nat. Commun.* **13**, 1538 (2022).
221. Zheng, Y., Jiao, Y., Vasileff, A. & Qiao, S. Z. The hydrogen evolution reaction in alkaline solution: from theory, single crystal models, to practical electrocatalysts. *Angew. Chem. Int. Ed.* **57**, 7568–7579 (2018).

222. Millet, P. & Grigoriev, S. in *Renewable Hydrogen Technologies* (eds Gandia, L. M., Arzamendi, G. & Dieguez, P. M.) 19–41 (Elsevier, 2013).
**This text presents an overview of mature and laboratory-scale water electrolysis technologies, and provides some common values of important process parameters, which helps put the process requirements in perspective**.
223. Burton, N. A., Padilla, R. V., Rose, A. & Habibullah, H. Increasing the efficiency of hydrogen production from solar powered water electrolysis. *Renew. Sustain. Energy Rev.* **135**, 110255 (2021).
224. Wang, M., Wang, Z., Gong, X. & Guo, Z. The intensification technologies to water electrolysis for hydrogen production — a review. *Renew. Sustain. Energy Rev.* **29**, 573–588 (2014).
225. Barati, G., Aliofkhazraei, M. & Shanmugam, S. Recent advances in methods and technologies for enhancing bubble detachment during electrochemical water splitting. *Renew. Sustain. Energy Rev.* **114**, 109300 (2019).
226. Rodríguez, J. & Amores, E. CFD modeling and experimental validation of an alkaline water electrolysis cell for hydrogen production. *Processes* **8**, 1634 (2020).
**This work introduces important engineering parameters that need to be taken into account when designing electrochemical cells**.
227. Knöppel, J. et al. On the limitations in assessing stability of oxygen evolution catalysts using aqueous model electrochemical cells. *Nat. Commun.* **12**, 1–9 (2021).
228. Watzele, S., Liang, Y. & Bandarenka, A. S. Intrinsic activity of some oxygen and hydrogen evolution reaction electrocatalysts under industrially relevant conditions. *ACS Appl. Energy Mater.* **1**, 4196–4202 (2018).
229. Lazaridis, T., Stühmeier, B. M., Gasteiger, H. A. & El-Sayed, H. A. Capabilities and limitations of rotating disk electrodes versus membrane electrode assemblies in the investigation of electrocatalysts. *Nat. Catal.* **5**, 363–373 (2022).
230. Scott, K. *Handbook of Industrial Membranes* 271–305 (Elsevier, 1995).
231. Wang, S. et al. Modifying ionic membranes with carbon dots enables direct production of high-purity hydrogen through water electrolysis. *ACS Appl. Mater. Interfaces* **13**, 39304–39310 (2021).
232. Ligen, Y., Vrubel, H. & Girault, H. Energy efficient hydrogen drying and purification for fuel cell vehicles. *Int. J. Hydrog. Energy* **45**, 10639–10647 (2020).
233. Akbashev, A. R. Electrocatalysis goes nuts. *ACS Catal.* **12**, 4296–4301 (2022).
234. Shinozaki, K., Zack, J. W., Richards, R. M., Pivovar, B. S. & Kocha, S. S. Oxygen reduction reaction measurements on platinum electrocatalysts utilizing rotating disk electrode technique: I. Impact of impurities, measurement protocols and applied corrections. *J. Electrochem. Soc.* **162**, F1144–F1158 (2015).
235. Christopher, P., Jin, S., Sivula, K. & Kamat, P. V. Why seeing is not always believing: common pitfalls in photocatalysis and electrocatalysis. *ACS Energy Lett.* **6**, 707–709 (2021).
236. McCrory, C. C. L., Jung, S., Peters, J. C. & Jaramillo, T. F. Benchmarking heterogeneous electrocatalysts for the oxygen evolution reaction. *J. Am. Chem. Soc.* **135**, 16977–16987 (2013).
**This work recommends a protocol to reliably compare the activity, stability, electrochemically active surface area and Faradic efficiency of electrocatalysts for the OER**.
237. Chen, J. G., Jones, C. W., Linic, S. & Stamenkovic, V. R. Best practices in pursuit of topics in heterogeneous electrocatalysis. *ACS Catal.* **7**, 6392–6393 (2017).
238. Bligaard, T. et al. Toward benchmarking in catalysis science: best practices, challenges, and opportunities. *ACS Catal.* **6**, 2590–2602 (2016).
239. Clark, E. L. et al. Standards and protocols for data acquisition and reporting for studies of the electrochemical reduction of carbon dioxide. *ACS Catal.* **8**, 6560–6570 (2018).
240. Kocha, S. S. et al. Best practices and testing protocols for benchmarking ORR activities of fuel cell electrocatalysts using rotating disk electrode. *Electrocatalysis* **8**, 366–374 (2017).
241. Anantharaj, S., Noda, S., Driess, M. & Menezes, P. W. The pitfalls of using potentiodynamic polarization curves for tafel analysis in electrocatalytic water splitting. *ACS Energy Lett.* **6**, 1607–1611 (2021).
242. Sheng, W., Gasteiger, H. A. & Shao-Horn, Y. Hydrogen oxidation and evolution reaction kinetics on platinum: acid vs alkaline electrolytes. *J. Electrochem. Soc.* **11**, B1529–B1536 (2010).
243. Lee, Y., Suntivich, J., May, K. J., Perry, E. E. & Shao-Horn, Y. Synthesis and activities of rutile $IrO_2$ and $RuO_2$ nanoparticles for oxygen evolution in acid and alkaline solutions. *J. Phys. Chem. L* **3**, 399–404 (2012).
244. Ku, H. H. Notes on the use of propagation of error formulas. *J. Res. Natl Bur. Stand.* **70C**, 263–273 (1966).
245. Payton, M. E., Greenstone, M. H. & Schenker, N. Overlapping confidence intervals or standard error intervals: what do they mean in terms of statistical significance? *J. Insect Sci.* **3**, 34 (2003).
246. Tummers, B. DataThief III. *DataThief* http://datathief.org (2006).
247. Rohatgi, A. WebPlotDigitizer version 4.3 https://automeris.io/WebPlotDigitizer/ (2020).
248. Flower, A., McKenna, J. W. & Upreti, G. Validity and reliability of GraphClick and DataThief III for data extraction. *Behav. Modif.* **40**, 396–413 (2015).
249. Govindarajan, N., Kastlunger, G., Heenen, H. H. & Chan, K. Improving the intrinsic activity of electrocatalysts for sustainable energy conversion: where are we and where can we go? *Chem. Sci.* **13**, 14–26 (2022).
250. Winther, K. T. et al. Catalysis-Hub.org, an open electronic structure database for surface reactions. *Sci. Data* **6**, 1–10 (2019).
251. Alvarez-Moreno, M. et al. Managing the computational chemistry big data problem: the ioChem-BD platform. *J. Chem. Inf. Model.* **55**, 95–103 (2015).
252. Hummelshøj, J. S., Abild-Pedersen, F., Studt, F., Bligaard, T. & Nørskov, J. K. CatApp: a web application for surface chemistry and heterogeneous catalysis. *Angew. Chem. Int. Ed.* **51**, 272–274 (2012).
253. Artrith, N. et al. Best practices in machine learning for chemistry. *Nat. Chem.* **13**, 505–508 (2021).
254. Tran, K. & Ulissi, Z. W. Active learning across intermetallics to guide discovery of electrocatalysts for $CO_2$ reduction and $H_2$ evolution. *Nat. Catal.* **1**, 696–703 (2018).
255. Zou, X. et al. Machine learning analysis and prediction models of alkaline anion exchange membranes for fuel cells. *Energy Environ. Sci.* **14**, 3965–3975 (2021).
256. Linpé, W. et al. Revisiting optical reflectance from Au(111) electrode surfaces with combined high-energy surface X-ray diffraction. *J. Electrochem. Soc.* **168**, 096511 (2021).
257. Resasco, J. et al. Enhancing the connection between computation and experiments in electrocatalysis. *Nat. Catal.* **5**, 374–381 (2022).
258. Witte, P. T. et al. BASF NanoSelect™ technology: innovative supported Pd- and Pt-based catalysts for selective hydrogenation reactions. *Top. Catal.* **55**, 505–511 (2012).
259. Tong, W. et al. Electrolysis of low-grade and saline surface water. *Nat. Energy* **5**, 367–377 (2020).
260. McAllister, B. & Hu, P. A density functional theory study of sulfur poisoning. *J. Chem. Phys.* **122**, 084709 (2005).
261. Akhade, S. A. et al. Poisoning effect of adsorbed CO during $CO_2$ electroreduction on late transition metals. *Phys. Chem. Chem. Phys.* **16**, 20429–20435 (2014).
262. Yang, G. et al. Interfacial engineering of $MoO_2$–FeP heterojunction for highly efficient hydrogen evolution coupled with biomass electrooxidation. *Adv. Mater.* **32**, 2000455 (2020).
263. Xie, Y., Zhou, Z., Yang, N. & Zhao, G. An overall reaction integrated with highly selective oxidation of 5-hydroxymethylfurfural and efficient hydrogen evolution. *Adv. Funct. Mater.* **31**, 2102886 (2021).
264. Wang, Z. et al. Copper–nickel nitride nanosheets as efficient bifunctional catalysts for hydrazine-assisted electrolytic hydrogen production. *Adv. Energy Mater.* **9**, 1900390 (2019).
265. Chen, Z., Wei, W., Song, L. & Ni, B. Hybrid water electrolysis: a new sustainable avenue for energy-saving hydrogen production. *Sustain. Horiz.* **1**, 100002 (2022).
**This work introduces fundamentals of hybrid water electrolysis and also provides examples of relevant anodic reactions and catalysts**.
266. Martínez, N. P., Isaacs, M. & Nanda, K. K. Paired electrolysis for simultaneous generation of synthetic fuels and chemicals. *New J. Chem.* **44**, 5617–5637 (2020).
267. Weinberg, N. L. & Weinberg, H. R. electrochemical oxidation of organic compounds. *Chem. Rev.* **68**, 449–523 (1968).
268. Xing, L. et al. Platinum electro-dissolution in acidic media upon potential cycling. *Electrocatalysis* **5**, 96–112 (2014).
269. Furuya, Y. et al. Influence of electrolyte composition and pH on platinum electrochemical and/or chemical dissolution in aqueous acidic media. *ACS Catal.* **5**, 2605–2614 (2015).
270. Edgington, J., Schweitzer, N., Alayoglu, S. & Seitz, L. C. Constant change: exploring dynamic oxygen evolution reaction catalysis and material transformations in strontium zinc iridate perovskite in acid. *J. Am. Chem. Soc.* **143**, 9961–9971 (2021).
271. Roy, C. et al. Trends in activity and dissolution on $RuO_2$ versus well-defined extended surfaces. *ACS Energy Lett.* **3**, 2045–2051 (2018).
272. Cherevko, S. Electrochemical dissolution of noble metals native oxides. *J. Electroanal. Chem.* **787**, 11–13 (2017).
273. Zhang, R. et al. A dissolution/precipitation equilibrium on the surface of iridium-based perovskites controls their activity as oxygen evolution reaction catalysts in acidic media. *Angew. Chem.* **131**, 4619–4623 (2019).
274. Seitz, L. C. et al. A highly active and stable $IrO_x/SrIrO_3$ catalyst for the oxygen evolution reaction. *Science* **353**, 1012–1014 (2016).
275. Aβmann, P., Gago, A. S., Gazdzicki, P., Friedrich, K. A. & Wark, M. Toward developing accelerated stress tests for proton exchange membrane electrolyzers. *Curr. Opin. Electrochem.* **21**, 225–233 (2020).
**This work discusses the importance of accelerated stress tests in the development of electrolysis technology**.
276. Iriawan, H. et al. Methods for nitrogen activation by reduction and oxidation. *Nat. Rev. Methods Primers* **1**, 1–26 (2021).
277. Clark, D. et al. Single-step hydrogen production from $NH_3$, $CH_4$, and biogas in stacked proton ceramic reactors. *Science* **376**, 390–393 (2022).
278. Lim, D.-K. et al. Solid acid electrochemical cell for the production of hydrogen from ammonia. *Joule* **4**, 2338–2347 (2020).
279. Shih, A. J. & Haile, S. M. Electrifying membranes to deliver hydrogen. *Science* **376**, 348–349 (2022).
280. Augustyn, V., Simon, P. & Dunn, B. Pseudocapacitive oxide materials for high-rate electrochemical energy storage. *Energy Environ. Sci.* **7**, 1597–1614 (2014).



### Acknowledgements
F.D. and N.L. thank the Spanish Ministry of Science and Innovation (RTI2018-101394-B-I00, Severo Ochoa CEX2019-000925-S). R.M. acknowledges the Dutch Organization for Scientific Research (NWO) for funding under grant number ECCM.TT.ECCM.001. A.H.M.d.S. and R.E.V. acknowledge the Materials Innovation Institute (M2i) and thank Tata Steel Nederland Technology BV and the Dutch Research Council (NWO) (project number ENPPS. IPP.019.002) for financial support. S.P. acknowledges support from the Basic Science Research Program through the National Research Foundation of Korea (NRF) funded by the Ministry of Education (2021R1A6A3A14039678). This project was also supported by the Solar-to-Products programme and the Advanced Research Center for Chemical Building Blocks (ARC CBBC) consortium, both co-financed by the NWO and by Shell Global Solutions B.V., and by the European Commission under contract 722614 (Innovative training network ELCoREL). The authors thank the invaluable peer reviewers who provided constructive comments.


### Author contributions
All authors researched data for the article. All authors contributed substantially to discussion of the content. A.J.S., M.C.O.M., F.D., D.P., M.P., A.H.M.d.S., R.E.V., K.O., S.P., O.v.d.H., G.M., A.G., M.V., G.T.K.K.G., R.M., N.L. and M.T.M.K. wrote the article. All authors reviewed and/or edited the manuscript before submission.

### Competing interests
The authors declare no competing interests.

### Peer review information
*Nature Reviews Methods Primers* thanks the anonymous reviewers for their contribution to the peer review of this work.

### Publisher's note
Springer Nature remains neutral with regard to jurisdictional claims in published maps and institutional affiliations.



### Supplementary information
The online version contains supplementary material available at https://doi.org/10.1038/s43586-022-00164-0.